A Novel Stretch Energy Minimization Algorithm for Equiareal Parameterizations

Mei-Heng Yueh · Wen-Wei Lin · Chin-Tien Wu · Shing-Tung Yau

Abstract Surface parameterizations have been widely applied to computer graphics and digital geometry processing. In this paper, we propose a novel stretch energy minimization (SEM) algorithm for the computation of equiareal parameterizations of simply connected open surfaces with very small area distortions and highly improved computational efficiencies. In addition, the existence of nontrivial limit points of the SEM algorithm is guaranteed under some mild assumptions of the mesh quality. Numerical experiments indicate that the accuracy, effectiveness, and robustness of the proposed SEM algorithm outperform the other state-of-the-art algorithms. Applications of the SEM on surface remeshing, registration and morphing for simply connected open surfaces are demonstrated thereafter. Thanks to the SEM algorithm, the computation for these applications can be carried out efficiently and reliably.

Keywords Equiareal parameterizations · Simply connected open surfaces · Surface remeshing · Surface registration

Mathematics Subject Classification (2000) 15B48 · 52C26 · 65F05 · 65F30

1 Introduction

A parameterization of a surface $\mathcal{M} \subset \mathbb{R}^3$ is a bijective mapping f that maps $\mathcal{M}$ to a planar region $\mathcal{D} \subset \mathbb{C}(\equiv \mathbb{R}^2)$. It has been widely applied to various tasks

Mei-Heng Yueh ✉
Department of Mathematics, National Taiwan Normal University, Teipei 11677, Taiwan
E-mail: yueh@math.ntnu.edu.tw

Wen-Wei Lin · Chin-Tien Wu
Department of Applied Mathematics, National Chiao Tung University, Hsinchu 300, Taiwan
E-mail: wwlin@math.nctu.edu.tw

Chin-Tien Wu
E-mail: ctw@math.nctu.edu.tw

Shing-Tung Yau
Department of Mathematics, Harvard University, Cambridge, MA 02138, USA
E-mail: yau@math.harvard.edu

of digital geometry processing, such as surface registration, resampling, remeshing, morphing, and texture mapping. Some classical methods and applications of surface parameterizations can be found in the survey papers [13,24,16].

The desired parameterization usually minimizes the distortion of angles [10, 29], areas or a mixture of them [22]. In particular, an area-preserving mapping is also called an equiareal parameterization. Some popular approaches for the computation of equiareal parameterizations are:

1. stretch-minimizing method [23,27],
2. Lie advection method [31],
3. optimal mass transportation method [11,15,30,25].

In applications of surface resampling and remeshing, a suitable parameterization can be applied so that the sampling on the surface in 3D space can be determined by the sampling on a planar domain of simple shapes via the one-to-one correspondence of the parameterization. The distortion of the sampling density between samplings on the surface and on the planar domain, respectively, is caused by the stretch of the parameterization. In order to control the density of the sampling on the surface via a planar domain, a parameterization with a very small stretch is required. One of the best options is the equiareal parameterization, which refers to as a bijective area-preserving mapping f that maps a surface $\mathcal{M} \subset \mathbb{R}^3$ onto a planar domain $\mathcal{D} \subset \mathbb{C}(= \mathbb{R}^2)$.

In computations, the surface we considered is a triangular mesh, i.e., a piecewise linear surface composed of triangles. A triangular mesh $\mathcal{M}$ in $\mathbb{R}^3$ is composed of triangular faces

$$\mathcal{F}(\mathcal{M}) = \{[v_i, v_j, v_k]\},$$

where, $v_i \equiv \left(v_i^1, v_i^2, v_i^3\right)^\top \in \mathbb{R}^3$ is a vertex of $\mathcal{M}$, the bracket $[v_1, \ldots, v_m]$ denotes the *convex hull* of the affinely independent points $\{v_1, \ldots, v_m\} \subset \mathbb{R}^3$ defined by

$$[v_1, \ldots, v_m] = \left\{ \sum_{\ell=1}^{m} \alpha_\ell v_\ell \,\middle|\, \sum_{\ell=1}^{m} \alpha_\ell = 1, \alpha_\ell \geq 0, \ell = 1, \ldots, m \right\} \subset \mathbb{R}^3.$$

For convenience, we denote the set of vertices of $\mathcal{M}$ by $\mathcal{V}(\mathcal{M})$ and the set of edges of $\mathcal{M}$ by

$$\mathcal{E}(\mathcal{M}) = \{[v_i, v_j] \mid [v_i, v_j, v_k] \in \mathcal{F}(\mathcal{M}) \text{ for some } v_k \in \mathcal{V}(\mathcal{M})\}.$$

1.1 Contributions

In this paper, we propose a novel stretch energy minimization (SEM) algorithm for the computation of disk-shaped equiareal parameterizations of simply connected open surfaces with small area distortions and highly improved computational efficiencies. The contributions can be divided into three folds. First, we improve the area distortion of the parameterization on a given surface $\mathcal{M}$ by introducing a novel iterative scheme of the SEM algorithm. The desired equiareal parameterization of $\mathcal{M}$ is achieved as the iteration converges. Second, the accuracy, effectiveness and robustness of the proposed SEM algorithm are highly improved compared with the other state-of-the-art algorithms. Third, we prove the existence of nontrivial (nonconstant) limit points of the SEM algorithm under some mild assumptions of the mesh quality.

1.2 Notations and Overview

The following notations are frequently used in this paper. Other notations will be clearly defined whenever they appear.

- Bold letters, e.g. $\mathbf{f}$, $\mathbf{g}$, $\mathbf{h}$, denote (complex) vectors.
- Capital letters, e.g. K, L, M, denote matrices.
- Typewriter letters, e.g. $\mathtt{I}$, $\mathtt{J}$, $\mathtt{K}$, denote ordered sets of indices.
- $\mathtt{I}(\ell)$ denotes the ℓ-th element of the ordered index set $\mathtt{I}$.
- $\mathbf{f}_i$ denotes the i-th entry of the vector $\mathbf{f}$.
- $\mathbf{f}_{\mathtt{I}}$ denotes the subvector of $\mathbf{f}$ composed of $\mathbf{f}_i$, for $i \in \mathtt{I}$.
- $|\mathbf{f}|$ denotes the vector with the i-th entry being $|\mathbf{f}_i|$.
- $\mathrm{diag}(\mathbf{f})$ denotes the diagonal matrix with the (i,i)-th entry being $\mathbf{f}_i$.
- $K_{i,j}$ denotes the (i,j)-th entry of the matrix K.
- $K_{\mathtt{I},\mathtt{J}}$ denotes the submatrix of K composed of $K_{i,j}$, for $i \in \mathtt{I}$ and $j \in \mathtt{J}$.
- $[u,v,w]$ denotes the triangular face with the vertices $\{u,v,w\} \subset \mathbb{R}^3$ or $\mathbb{C}$.
- $|[u,v,w]|$ denotes the area of the triangular face $[u,v,w]$.
- i denotes the imaginary unit $\sqrt{-1}$.
- n_K denotes the number of rows of a squared matrix K.
- $n_{\mathtt{I}}$ denotes the number of elements of an ordered index set $\mathtt{I}$.
- I_n denotes the identity matrix of size $n \times n$.
- $\mathbf{1}_n$ denotes the vector of length n with all entries being one.
- $\mathbf{0}$ denotes the zero vectors and matrices of appropriate sizes.

This paper is organized as follows. First, the discrete equiareal parameterization and a brief review of the most related work on the fast stretch minimization are introduced in Sect. 2 and 3, respectively. Then the SEM algorithm for the computation of equiareal parameterizations of simply connected open surfaces is proposed in Sect. 5. The proof of the existence of nontrivial limit points for the SEM algorithm is given in Sect. 6. Numerical results of the SEM algorithm compared with two state-of-the-art methods [27,25] are presented in Sect. 7. Finally, some applications of the SEM algorithm on surface remeshing and surface registration are demonstrated in Sect. 8. A concluding remark is given in Sect. 9.

2 Discrete Equiareal Mappings

Given a triangular mesh $\mathcal{M}$ of n vertices $\{v_\ell\}_{\ell=1}^n$ with $v_\ell \in \mathbb{R}^3$. A bijective piecewise affine mapping f from $\mathcal{M}$ to a unit disk $\mathbb{D}$: $f : \mathcal{M} \to \mathbb{D} \subset \mathbb{C}$ can be expressed by a complex-valued vector

$$\mathbf{f} = (\mathbf{f}_1, \dots \mathbf{f}_n)^\top \in \mathbb{C}^n,$$

where $\mathbf{f}_\ell = f(v_\ell)$, for $\ell = 1, \dots, n$. For convenience, we write $\mathbf{f}_\ell = \mathbf{f}_\ell^1 + \mathrm{i}\mathbf{f}_\ell^2$, where $\mathbf{f}_\ell^1$, $\mathbf{f}_\ell^2 \in \mathbb{R}$, for $\ell = 1, \dots, n$. For $z \in [\mathbf{f}_i, \mathbf{f}_j, \mathbf{f}_k] \subset \mathbb{D}$, the inverse mapping $f^{-1} : \mathbb{D} \to \mathcal{M}$ is defined by

$$f^{-1}\big|_{[\mathbf{f}_i,\mathbf{f}_j,\mathbf{f}_k]}(z) = \frac{|[z,\mathbf{f}_j,\mathbf{f}_k]|v_i + |[\mathbf{f}_i,z,\mathbf{f}_k]|v_j + |[\mathbf{f}_i,\mathbf{f}_j,z]|v_k}{|[\mathbf{f}_i,\mathbf{f}_j,\mathbf{f}_k]|}, \tag{1}$$

where $|[\mathbf{f}_i,\mathbf{f}_j,\mathbf{f}_k]|$ denotes the area of the triangle $[\mathbf{f}_i,\mathbf{f}_j,\mathbf{f}_k]$ given by

$$|[\mathbf{f}_i,\mathbf{f}_j,\mathbf{f}_k]| = \frac{1}{2}\left|(\mathbf{f}_i^1 - \mathbf{f}_k^1)(\mathbf{f}_j^2 - \mathbf{f}_k^2) - (\mathbf{f}_i^2 - \mathbf{f}_k^2)(\mathbf{f}_j^1 - \mathbf{f}_k^1)\right|. \tag{2}$$

Let $z = z^1 + \mathrm{i}z^2$, $z^1, z^2 \in \mathbb{R}$. From (1) and (2), the partial derivatives of f^{-1} with respect to z^1 and z^2 can be expressed by

$$\frac{\partial f^{-1}\big|_{[\mathbf{f}_i,\mathbf{f}_j,\mathbf{f}_k]}}{\partial z^1}(z) = \frac{1}{2|[\mathbf{f}_i,\mathbf{f}_j,\mathbf{f}_k]|}\left[(\mathbf{f}_j^2 - \mathbf{f}_k^2)v_i + (\mathbf{f}_k^2 - \mathbf{f}_i^2)v_j + (\mathbf{f}_i^2 - \mathbf{f}_j^2)v_k\right]$$

and

$$\frac{\partial f^{-1}\big|_{[\mathbf{f}_i,\mathbf{f}_j,\mathbf{f}_k]}}{\partial z^2}(z) = \frac{1}{2|[\mathbf{f}_i,\mathbf{f}_j,\mathbf{f}_k]|}\left[(\mathbf{f}_k^1 - \mathbf{f}_j^1)v_i + (\mathbf{f}_i^1 - \mathbf{f}_k^1)v_j + (\mathbf{f}_j^1 - \mathbf{f}_i^1)v_k\right],$$

respectively. The discrete first fundamental form of f^{-1} is defined as

$$I_{f^{-1}}(z) = \left[J_{f^{-1}}(z)\right]^\top \left[J_{f^{-1}}(z)\right], \tag{3}$$

where $J_{f^{-1}}(z) = \left[\frac{\partial f^{-1}}{\partial z^1}(z)\ \frac{\partial f^{-1}}{\partial z^2}(z)\right]$ is the Jacobian matrix of f^{-1}. A bijective mapping $f : \mathcal{M} \to \mathbb{D}$ is said to be equiareal if

$$\det\left(I_{f^{-1}}(z)\right) = c,$$

for some constant c, for every $z \in \mathbb{D}$.

3 Previous Works

In this section, we briefly review the fast stretch minimization (FSM) algorithm [27] with the discrete harmonic map [12] as the initial mapping for the computation of an equiareal parameterization of a simply connected open mesh $\mathcal{M}$ proposed by Yoshizawa et al., which is the most related work. The computational procedure of FSM [27] is described as follows.

3.1 Discrete Harmonic Mappings

Given a simply connected open mesh $\mathcal{M}$, the discrete harmonic mapping is the minimizer of the discrete Dirichlet energy

$$E_D(f) = \frac{1}{2}\sum_{[v_i,v_j]\in\mathcal{E}(\mathcal{M})} w_{i,j}\left|f(v_i) - f(v_j)\right|^2, \tag{4}$$

where $w_{i,j}$ is the cotangent weight on the edge $[v_i, v_j]$ defined by

$$w_{i,j} = \frac{\cot\alpha_{i,j} + \cot\alpha_{j,i}}{2} \tag{5}$$

in which $\alpha_{i,j}$ and $\alpha_{j,i}$ are two angles opposite to the edge $[v_i, v_j]$, as illustrated in Fig. 1. The energy functional (4) can be written as

$$E_D(f) = \frac{1}{2}\mathbf{f}^* L\mathbf{f},$$

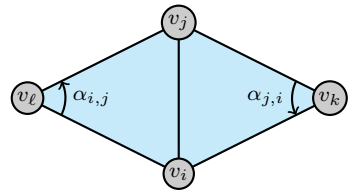

Fig. 1 An illustration for the cotangent weights.

where $\mathbf{f} = (f(v_1), \ldots, f(v_n))^\top$, $\mathbf{f}^*$ denotes the conjugate transpose of $\mathbf{f}$, and L is the Laplacian matrix defined by

$$L_{i,j} = \begin{cases} -w_{i,j} & \text{if } [v_i, v_j] \in \mathcal{E}(\mathcal{M}), \\ \sum_{k \neq i} w_{i,k} & \text{if } j = i, \\ 0 & \text{otherwise.} \end{cases} \tag{6}$$

Suppose $\mathtt{I}$ and $\mathtt{B}$ are the sets of indices of interior vertices and boundary vertices, respectively. The discrete harmonic mapping can be computed by solving the discrete Laplace-Beltrami equation

$$L_{\mathtt{I},\mathtt{I}}\mathbf{f}_{\mathtt{I}} = -L_{\mathtt{I},\mathtt{B}}\mathbf{f}_{\mathtt{B}},$$

where $\mathbf{f}_{\mathtt{B}}$ is the boundary mapping given by $\mathbf{f}_{\mathtt{B}(j)} = \cos\theta_j + \mathrm{i}\sin\theta_j$, in which $\theta_j = 2\pi \frac{\sum_{\ell=1}^{j} |v_{\mathtt{B}(\ell+1)} - v_{\mathtt{B}(\ell)}|}{\sum_{\ell=1}^{n_{\mathtt{B}}} |v_{\mathtt{B}(\ell+1)} - v_{\mathtt{B}(\ell)}|}$, and $v_{\mathtt{B}(n_{\mathtt{B}}+1)} := v_{\mathtt{B}(1)}$, for $j = 1, \ldots, n_{\mathtt{B}}$.

3.2 Iterative Scheme of the FSM Algorithm

Given a bijective piecewise affine mapping $f : \mathcal{M} \to \mathbb{D} \subset \mathbb{C}$. Let $\gamma^{\pm}_{f^{-1}}(z)$ be two singular values of the Jacobian matrix $J_{f^{-1}}(z) = \left[\frac{\partial f^{-1}}{\partial z^1}(z)\ \frac{\partial f^{-1}}{\partial z^2}(z)\right]$. Note that $\gamma^{\pm}_{f^{-1}}|_\tau(z)$ is constant on each triangular face $\tau \in \mathcal{F}(\mathcal{M})$. The *stretch metric* over τ is defined as

$$\mathcal{S}_{f^{-1}}(\tau) = \sqrt{\frac{(\gamma^{+}_{f^{-1}}|_\tau)^2 + (\gamma^{-}_{f^{-1}}|_\tau)^2}{2}} = \sqrt{\frac{a_{f^{-1}}|_\tau + c_{f^{-1}}|_\tau}{2}}, \tag{7}$$

where $a_{f^{-1}}|_\tau = (\frac{\partial f^{-1}}{\partial z^1})^\top (\frac{\partial f^{-1}}{\partial z^1})|_\tau$ and $c_{f^{-1}}|_\tau = (\frac{\partial f^{-1}}{\partial z^2})^\top (\frac{\partial f^{-1}}{\partial z^2})|_\tau$, i.e., the root-mean-square of the singular values of $J_{f^{-1}}$ [23]. Then the stretch metric on the vertex v_j is defined as

$$\mathcal{T}_{f^{-1}}(v_j) = \sqrt{\frac{\sum_{\tau \in \mathcal{N}(v_j)} |\tau| \mathcal{S}_{f^{-1}}(\tau)^2}{\sum_{\tau \in \mathcal{N}(v_j)} |\tau|}}, \tag{8}$$

in which $\mathcal{N}(v_j) = \{\tau \in \mathcal{F}(\mathcal{M}) \,|\, v_j \in \tau\}$, and $|\tau|$ denotes the area of the triangular face $\tau \in \mathcal{F}(\mathcal{M})$.

Recall that the initial mapping $f^{(0)}$ in the FSM algorithm [27] is a disk-shaped harmonic mapping stated in Sect. 3.1. Then interior vertices of the mapping $f^{(k)}$ are updated via redistributing local stretches by $w_{i,j}^{(0)} := w_{i,j}$ and

$$w_{i,j}^{(k)} = \frac{w_{i,j}^{(k-1)}}{\mathcal{T}_{(f^{(k-1)})^{-1}}(v_j)},$$

where $\mathcal{T}_{(f^{(k-1)})^{-1}}$ is defined in (8). In other words, if we let the weight matrix $W^{(k)}$ be

$$W_{i,j}^{(k)} = \begin{cases} w_{i,j}^{(k)} & \text{if } [v_i, v_j] \in \mathcal{E}(\mathcal{M}), \\ 0 & \text{otherwise,} \end{cases}$$

then the interior vertices $\mathbf{f}_{\mathtt{I}}$ is updated by the iteration

$$L_{\mathtt{I},\mathtt{I}}^{(k)} \mathbf{f}_{\mathtt{I}}^{(k)} = -L_{\mathtt{I},\mathtt{B}}^{(k)} \mathbf{f}_{\mathtt{B}}, \tag{9}$$

where $\mathbf{f}_{\mathtt{I}}^{(0)} \equiv \mathbf{f}_{\mathtt{I}}$, $L^{(0)} \equiv L$ as in (6), and

$$L^{(k)} = \operatorname{diag}\left(\left[\sum_{j=1}^{n} W_{i,j}^{(k)} \right]_{i=1}^{n} \right) - W^{(k)}.$$

Note that the FSM algorithm [27] has the following drawbacks, namely, (i) the stretch metric (7) cannot distinguish some different types of the first fundamental forms, e.g.,

$$\begin{bmatrix} 1 & 0 \\ 0 & 1 \end{bmatrix}, \quad \begin{bmatrix} 1.2 & 0 \\ 0 & 0.8 \end{bmatrix}, \quad \text{and} \quad \begin{bmatrix} 1 & 0.3 \\ 0.2 & 1 \end{bmatrix};$$

(ii) The matrix $L_{\mathtt{I},\mathtt{I}}^{(k)}$ in the linear system (9), in general, is not symmetric; (iii) The mapping of boundary vertices in the FSM algorithm is completely determined by the initial mapping.

4 The Stretch Factor

To remedy the drawback of the stretch metric in the FSM algorithm, we introduce the *stretch factor* in (10) which will be used in our proposed algorithm. Given a mesh $\mathcal{M}$ with a parameterization $f : \mathcal{M} \to \mathbb{D} \subset \mathbb{C}$, the *stretch factor* $\sigma_{f^{-1}} : \mathcal{F}(\mathcal{M}) \to \mathbb{R}$ with respect to f^{-1} is defined by

$$\sigma_{f^{-1}}(\tau) = \frac{|\tau|}{|f(\tau)|}, \tag{10}$$

where $|\tau|$ and $|f(\tau)|$ denote the areas of the triangular face τ and its image $f(\tau)$, respectively. In fact, the stretch factor (10) is exactly the square root of the determinant of the discrete first fundamental form in (3).

Theorem 1 *Given a mesh $\mathcal{M}$ and a parameterization mapping $f : \mathcal{M} \to \mathbb{D} \subset \mathbb{C}$. The stretch factor $\sigma_{f^{-1}}$, defined in (10), satisfies*

$$\sigma_{f^{-1}}(\tau) = \sqrt{\det\left(I_{f^{-1}}\big|_{f(\tau)}\right)}, \tag{11}$$

for every $\tau \in \mathcal{F}(\mathcal{M})$.

Proof We write $\mathbf{f} = (\mathbf{f}_1, \ldots, \mathbf{f}_n)^\top := (f(v_1), \ldots, f(v_n))^\top \in \mathbb{C}^n$, where $\mathbf{f}_\ell = f(v_\ell)$, for $\ell = 1 \ldots, n$. Note that the partial derivatives are translation invariant. Without loss of generality, let $v_i + v_j + v_k = 0$, and $\mathbf{f}_i + \mathbf{f}_j + \mathbf{f}_k = 0$. That is, $v_k = -v_i - v_j$, and $\mathbf{f}_k = -\mathbf{f}_i - \mathbf{f}_j$. A direct computation yields that

$$|[\mathbf{f}_i, \mathbf{f}_j, \mathbf{f}_k]| = \frac{3}{2} \left| \mathbf{f}_i^1 \mathbf{f}_j^2 - \mathbf{f}_i^2 \mathbf{f}_j^1 \right|.$$

Similarly,

$$\begin{aligned} |[v_i, v_j, v_k]|^2 &= \frac{1}{4} \|(v_i - v_k) \times (v_j - v_k)\|^2 = \frac{1}{4} \|(2v_i + v_j) \times (v_i + 2v_j)\|^2 \\ &= \frac{1}{4} \left(\|2v_i + v_j\|^2 \|v_i + 2v_j\|^2 - ((2v_i + v_j)^\top (v_i + 2v_j))^2 \right) \\ &= \frac{9}{4} \left((v_i^\top v_i)(v_j^\top v_j) - (v_i^\top v_j)^2 \right). \end{aligned}$$

On the other hand,

$$\frac{\partial f^{-1} \big|_{[\mathbf{f}_i, \mathbf{f}_j, \mathbf{f}_k]}}{\partial z^1} = \frac{\mathbf{f}_j^2 v_i - \mathbf{f}_i^2 v_j}{\left| \mathbf{f}_i^1 \mathbf{f}_j^2 - \mathbf{f}_i^2 \mathbf{f}_j^1 \right|} \quad \text{and} \quad \frac{\partial f^{-1} \big|_{[\mathbf{f}_i, \mathbf{f}_j, \mathbf{f}_k]}}{\partial z^2} = \frac{\mathbf{f}_i^1 v_j - \mathbf{f}_j^1 v_i}{\left| \mathbf{f}_i^1 \mathbf{f}_j^2 - \mathbf{f}_i^2 \mathbf{f}_j^1 \right|}.$$

Hence,

$$\begin{aligned} a_{f^{-1}} \big|_{[\mathbf{f}_i, \mathbf{f}_j, \mathbf{f}_k]} &= \left(\frac{\partial f^{-1} \big|_{[\mathbf{f}_i, \mathbf{f}_j, \mathbf{f}_k]}}{\partial z^1} \right)^\top \left(\frac{\partial f^{-1} \big|_{[\mathbf{f}_i, \mathbf{f}_j, \mathbf{f}_k]}}{\partial z^1} \right) \\ &= \frac{(\mathbf{f}_j^2)^2 (v_i^\top v_i) - 2\mathbf{f}_1^2 \mathbf{f}_j^2 (v_i^\top v_j) + (\mathbf{f}_i^2)^2 (v_j^\top v_j)}{\left| \mathbf{f}_i^1 \mathbf{f}_j^2 - \mathbf{f}_i^2 \mathbf{f}_j^1 \right|}, \end{aligned}$$

$$\begin{aligned} b_{f^{-1}} \big|_{[\mathbf{f}_i, \mathbf{f}_j, \mathbf{f}_k]} &= \left(\frac{\partial f^{-1} \big|_{[\mathbf{f}_i, \mathbf{f}_j, \mathbf{f}_k]}}{\partial z^1} \right)^\top \left(\frac{\partial f^{-1} \big|_{[\mathbf{f}_i, \mathbf{f}_j, \mathbf{f}_k]}}{\partial z^2} \right) \\ &= \frac{-\mathbf{f}_j^1 \mathbf{f}_j^2 (v_i^\top v_i) + (\mathbf{f}_i^1 \mathbf{f}_j^2 + \mathbf{f}_i^2 \mathbf{f}_j^1)(v_i^\top v_j) - \mathbf{f}_i^1 \mathbf{f}_i^2 (v_j^\top v_j)}{\left| \mathbf{f}_i^1 \mathbf{f}_j^2 - \mathbf{f}_i^2 \mathbf{f}_j^1 \right|}, \end{aligned}$$

and

$$\begin{aligned} c_{f^{-1}} \big|_{[\mathbf{f}_i, \mathbf{f}_j, \mathbf{f}_k]} &= \left(\frac{\partial f^{-1} \big|_{[\mathbf{f}_i, \mathbf{f}_j, \mathbf{f}_k]}}{\partial z^2} \right)^\top \left(\frac{\partial f^{-1} \big|_{[\mathbf{f}_i, \mathbf{f}_j, \mathbf{f}_k]}}{\partial z^2} \right) \\ &= \frac{(\mathbf{f}_j^1)^2 (v_i^\top v_i) - 2\mathbf{f}_1^1 \mathbf{f}_j^1 (v_i^\top v_j) + (\mathbf{f}_i^1)^2 (v_j^\top v_j)}{\left| \mathbf{f}_i^1 \mathbf{f}_j^2 - \mathbf{f}_i^2 \mathbf{f}_j^1 \right|}. \end{aligned}$$

It follows that

$$\begin{aligned}
\det\left(I_{f^{-1}}\big|_{[\mathbf{f}_i,\mathbf{f}_j,\mathbf{f}_k]}\right) &= a_{f^{-1}}\big|_{[\mathbf{f}_i,\mathbf{f}_j,\mathbf{f}_k]}\, c_{f^{-1}}\big|_{[\mathbf{f}_i,\mathbf{f}_j,\mathbf{f}_k]} - \left(b_{f^{-1}}\big|_{[\mathbf{f}_i,\mathbf{f}_j,\mathbf{f}_k]}\right)^2 \\
&= \frac{(\mathbf{f}_i^1\mathbf{f}_j^2 - \mathbf{f}_i^2\mathbf{f}_j^1)^2\left((v_i^\top v_i)(v_j^\top v_j) - (v_i^\top v_j)^2\right)}{\left|\mathbf{f}_i^1\mathbf{f}_j^2 - \mathbf{f}_i^2\mathbf{f}_j^1\right|^4} \\
&= \frac{(v_i^\top v_i)(v_j^\top v_j) - (v_i^\top v_j)^2}{\left|\mathbf{f}_i^1\mathbf{f}_j^2 - \mathbf{f}_i^2\mathbf{f}_j^1\right|^2} \\
&= \frac{\frac{9}{4}\left((v_i^\top v_i)(v_j^\top v_j) - (v_i^\top v_j)^2\right)}{\left(\frac{3}{2}\left|\mathbf{f}_i^1\mathbf{f}_j^2 - \mathbf{f}_i^2\mathbf{f}_j^1\right|\right)^2} \\
&= \frac{|[v_i,v_j,v_k]|^2}{|[\mathbf{f}_i,\mathbf{f}_j,\mathbf{f}_k]|^2} = \sigma_{f^{-1}}([v_i,v_j,v_k])^2.
\end{aligned}$$

Therefore, (11) follows directly by the positivity of the stretch factor. □

From (3) follows Corollary 1 immediately.

Corollary 1 *The value of $\sigma_{f^{-1}}(\tau)$ is the product of the singular values of the Jacobian matrix $J_{f^{-1}}\big|_{f(\tau)}$, for every $\tau \in \mathcal{F}(\mathcal{M})$.*

Our goal for the computation of equiareal parameterization is to find a bijective mapping $f : \mathcal{M} \to \mathbb{D}$ having the property that $\sigma_{f^{-1}}$ is constant.

5 The Stretch Energy Minimization Algorithm

In this section, we describe the SEM algorithm for the computation of an equiareal parameterization f of a simply connected open surface $\mathcal{M}$. First, the *stretch energy* is introduced in Sect. 5.1. Then the iterative scheme of the SEM algorithm is proposed in Sect. 5.2 for achieving the equiareal parameterization.

5.1 The Stretch Energy

Given a mesh $\mathcal{M}$ with a parameterization $f : \mathcal{M} \to \mathbb{D} \subset \mathbb{C}$. Note that the cotangent formula (5) can be written as

$$w_{i,j} = \frac{1}{2}\sum_{[v_i,v_j,v_k]\in\mathcal{F}(\mathcal{M})} \frac{(v_i - v_k)^\top (v_j - v_k)}{2|[v_i,v_j,v_k]|},$$

where the numerator and the denominator contain the angle and area information of the triangular mesh $\mathcal{M}$, respectively. In order to relax the angular constraints while retaining the area information, we modify the weight $w_{i,j}$ to $w_{i,j}(f)$ by

$$w_{i,j}(f) = \frac{1}{2}\sum_{[v_i,v_j,v_k]\in\mathcal{F}(\mathcal{M})} \frac{(f(v_i) - f(v_k))^* (f(v_j) - f(v_k))}{2\,|[v_i,v_j,v_k]|}. \tag{12}$$

Equivalently, the modified weight (12) can be written as

$$\begin{aligned} w_{i,j}(f) &= \frac{1}{2} \sum_{[v_i,v_j,v_k]\in\mathcal{F}(\mathcal{M})} \frac{(f(v_i)-f(v_k))^* (f(v_j)-f(v_k))}{2\,|f([v_i,v_j,v_k])|\,\sqrt{\det\left(I_{f^{-1}}\,|_{f([v_i,v_j,v_k])}\right)}} \\ &= \frac{1}{2} \sum_{[v_i,v_j,v_k]\in\mathcal{F}(\mathcal{M})} \frac{(f(v_i)-f(v_k))^* (f(v_j)-f(v_k))}{2\,|f([v_i,v_j,v_k])|\,\sigma_{f^{-1}}([v_i,v_j,v_k])} \\ &= \frac{1}{2} \sum_{[v_i,v_j,v_k]\in\mathcal{F}(\mathcal{M})} \frac{\cot(\alpha_{i,j}(f))}{\sigma_{f^{-1}}([v_i,v_j,v_k])}, \end{aligned} \tag{13}$$

where $\sigma_{f^{-1}}$ is the stretch factor defined in (10), $\alpha_{i,j}(f)$ is the angle at $f(v_k)$ opposite to the edge $f([v_i,v_j])$ connecting points $f(v_i)$ and $f(v_j)$ on $\mathbb{C}$. The modified Laplacian matrix $L(f)$ is defined as

$$[L(f)]_{i,j} = \begin{cases} -w_{i,j}(f) & \text{if } [v_i,v_j]\in\mathcal{E}(\mathcal{M}), \\ \sum_{\ell\neq i} w_{i,\ell}(f) & \text{if } j=i, \\ 0 & \text{otherwise.} \end{cases} \tag{14}$$

where $w_{i,j}(f)$ is given in (13) and the *stretch energy* is now defined by

$$E_S(f) = \frac{1}{2}\mathbf{f}^* L(f)\mathbf{f}. \tag{15}$$

5.2 Iterative Scheme of the SEM Algorithm

Our aim is to find a minimizer for the stretch energy functional (15). Note that $\mathbf{f}_\ell = \mathbf{f}_\ell^1 + \mathrm{i}\mathbf{f}_\ell^2$ in which $\mathbf{f}_\ell^1, \mathbf{f}_\ell^2 \in \mathbb{R}$, for $\ell = 1,\ldots,n$. The stretch energy (15) can be written as

$$E_S(\mathbf{f}^1,\mathbf{f}^2) = \frac{1}{2}\left((\mathbf{f}^1)^\top L(f)\mathbf{f}^1 + (\mathbf{f}^2)^\top L(f)\mathbf{f}^2\right).$$

Then the gradient

$$\nabla E_S(\mathbf{f}^1,\mathbf{f}^2) = \left(\frac{\partial E_S(\mathbf{f}^1,\mathbf{f}^2)}{\partial \mathbf{f}^1}, \frac{\partial E_S(\mathbf{f}^1,\mathbf{f}^2)}{\partial \mathbf{f}^2}\right)$$

of the energy functional can be calculated by

$$\frac{\partial E_S(\mathbf{f}^1,\mathbf{f}^2)}{\partial \mathbf{f}^s} = L(f)\mathbf{f}^s + \frac{1}{2}\sum_{t=1}^{2}(\mathbf{f}^t)^\top \frac{\partial L(f)}{\partial \mathbf{f}^s}\mathbf{f}^t, \tag{16}$$

where $\frac{\partial L(f)}{\partial \mathbf{f}^s}$ is the tensor with entries as

$$\frac{\partial [L(f)]_{i,j}}{\partial \mathbf{f}_k^s} = \begin{cases} -\frac{1}{2}\displaystyle\sum_{[v_i,v_j,v_\ell]\in\mathcal{F}(\mathcal{M})} \frac{\mathbf{f}_j^s - \mathbf{f}_\ell^s}{2|[v_i,v_j,v_\ell]|} & \text{if } [v_i,v_j]\in\mathcal{E}(\mathcal{M}),\ k=i, \\ -\frac{1}{2}\displaystyle\sum_{[v_i,v_j,v_\ell]\in\mathcal{F}(\mathcal{M})} \frac{\mathbf{f}_i^s - \mathbf{f}_\ell^s}{2|[v_i,v_j,v_\ell]|} & \text{if } [v_i,v_j]\in\mathcal{E}(\mathcal{M}),\ k=j, \\ -\frac{1}{2}\dfrac{2\mathbf{f}_k^s - \mathbf{f}_i^s - \mathbf{f}_j^s}{2|[v_i,v_j,v_k]|} & \text{if } [v_i,v_j,v_k]\in\mathcal{F}(\mathcal{M}), \\ 0 & \text{otherwise,} \end{cases}$$

for $s = 1, 2$. A direct computation yields that

$$\left[(\mathbf{f}^s)^\top \frac{\partial L(f)}{\partial \mathbf{f}^s}\right]_{j,k} = \begin{cases} -\frac{1}{2} \displaystyle\sum_{[v_\alpha, v_j, v_k] \in \mathcal{F}(\mathcal{M})} \frac{(\mathbf{f}_k^s - \mathbf{f}_\alpha^s)(\mathbf{f}_\alpha^s - \mathbf{f}_j^s)}{2|[v_\alpha, v_j, v_k]|} & \text{if } [v_j, v_k] \in \mathcal{E}(\mathcal{M}), \\ -\frac{1}{2} \displaystyle\sum_{[v_\alpha, v_j, v_\beta] \in \mathcal{F}(\mathcal{M})} \frac{(\mathbf{f}_\alpha^s - \mathbf{f}_\beta^s)^2}{2|[v_\alpha, v_j, v_\beta]|} & \text{if } k = j, \\ 0 & \text{otherwise,} \end{cases} \tag{17}$$

for $s = 1, 2$. Similarly,

$$\left[(\mathbf{f}^s)^\top \frac{\partial L(f)}{\partial \mathbf{f}^t}\right]_{j,k} = \begin{cases} -\frac{1}{2} \displaystyle\sum_{[v_\alpha, v_j, v_k] \in \mathcal{F}(\mathcal{M})} \frac{2(\mathbf{f}_k^s - \mathbf{f}_\alpha^s)(\mathbf{f}_\alpha^t - \mathbf{f}_j^t) - (\mathbf{f}_j^s - \mathbf{f}_\alpha^s)(\mathbf{f}_\alpha^t - \mathbf{f}_k^t)}{2|[v_\alpha, v_j, v_k]|} & \text{if } [v_j, v_k] \in \mathcal{E}(\mathcal{M}), \\ -\frac{1}{2} \displaystyle\sum_{[v_\alpha, v_j, v_\beta] \in \mathcal{F}(\mathcal{M})} \frac{(\mathbf{f}_\alpha^s - \mathbf{f}_\beta^s)(\mathbf{f}_\alpha^t - \mathbf{f}_\beta^t)}{2|[v_\alpha, v_j, v_\beta]|} & \text{if } k = j, \\ 0 & \text{otherwise,} \end{cases} \tag{18}$$

for $(s, t) = (1, 2), (2, 1)$. The derivations of (17) and (18) can be found in Appendix A for details.

To simplify the calculation, in practice, we omit the quadratic terms in (16) and propose the iterative scheme for equiareal parameterizations as follows. First, the initial map $\mathbf{f}^{(0)}$ is given by the harmonic map [12] in Sect. 3.1. Then the mapping of boundary vertices is updated by solving the linear system

$$\left[L(f^{(k)})\right]_{\mathtt{B},\mathtt{B}} \mathbf{f}_{\mathtt{B}}^{(k+1)} = -\left[L(f^{(k)})\right]_{\mathtt{B},\mathtt{I}} \mathbf{f}_{\mathtt{I}}^{(k)}. \tag{19}$$

To ensure that boundary vertices are mapped on the unit circle, we centralize the mapping by

$$\mathbf{f}_{\mathtt{B}}^{(k+1)} \leftarrow \left(I_{n_{\mathtt{B}}} - \frac{\mathbf{1}_{n_{\mathtt{B}}} \mathbf{1}_{n_{\mathtt{B}}}^\top}{n_{\mathtt{B}}}\right) \mathbf{f}_{\mathtt{B}}^{(k+1)}, \tag{20}$$

and normalize the mapping by

$$\mathbf{f}_{\mathtt{B}}^{(k+1)} \leftarrow \mathrm{diag}\left(\left|\mathbf{f}_{\mathtt{B}}^{(k+1)}\right|^{-1}\right) \mathbf{f}_{\mathtt{B}}^{(k+1)}. \tag{21}$$

Finally, the mapping of interior vertices is updated by solving the linear system

$$\left[L(f^{(k)})\right]_{\mathtt{I},\mathtt{I}} \mathbf{f}_{\mathtt{I}}^{(k+1)} = -\left[L(f^{(k)})\right]_{\mathtt{I},\mathtt{B}} \mathbf{f}_{\mathtt{B}}^{(k+1)}. \tag{22}$$

Equivalently, the iterations (19)-(22) can be written as

$$\mathbf{f}_{\mathtt{B}}^{(k+1)} = N^{(k)} C K^{(k)} \mathbf{f}_{\mathtt{B}}^{(k)} \tag{23}$$

with

$$K^{(0)} = \left[L(f^{(0)})\right]_{\mathtt{B},\mathtt{B}}^{-1} \left[L(f^{(0)})\right]_{\mathtt{B},\mathtt{I}} L_{\mathtt{I},\mathtt{I}}^{-1} L_{\mathtt{I},\mathtt{B}}$$

and

$$K^{(k)} = \left[L(f^{(k)})\right]_{\mathtt{B},\mathtt{B}}^{-1} \left[L(f^{(k)})\right]_{\mathtt{B},\mathtt{I}} \left[L(f^{(k-1)})\right]_{\mathtt{I},\mathtt{I}}^{-1} \left[L(f^{(k-1)})\right]_{\mathtt{I},\mathtt{B}},$$

for $k \in \mathbb{N}$, C and $N^{(k)}$ are the centralization and normalization matrices, respectively, given by

$$C = I_{n_{\mathtt{B}}} - \frac{\mathbf{1}_{n_{\mathtt{B}}} \mathbf{1}_{n_{\mathtt{B}}}^{\top}}{n_{\mathtt{B}}}$$

and

$$N^{(k)} = \operatorname{diag}\left(\left| C \left[L(f^{(k)})\right]_{\mathtt{B},\mathtt{B}}^{-1} \left[L(f^{(k)})\right]_{\mathtt{B},\mathtt{I}} \mathbf{f}_{\mathtt{I}}^{(k)} \right|^{-1} \right).$$

Remark 1 The matrices $[L(\mathbf{f}^{(k)})]_{\mathtt{B},\mathtt{B}}$ and $[L(\mathbf{f}^{(k)})]_{\mathtt{I},\mathtt{I}}$ in (19) and (22), respectively, are symmetric positive definite so that the Cholesky decompositions can be applied to solving linear systems conveniently in steps 3, 7 and 10 in Algorithm 1.

Remark 2 Several experiments indicate that the resulting equiareal parameterization would be slightly improved by performing an inversion transformation

$$\mathbf{f}_{\mathtt{I}(\ell)}^{(k)} \leftarrow \frac{1}{\left(\mathbf{f}_{\mathtt{I}(\ell)}^{(k)}\right)^*},$$

for $\ell = 1, \ldots, n_{\mathtt{I}}$, before solving the linear system (19). In other words, Eq. (19) is replaced by the equation

$$\left[L(f^{(k)})\right]_{\mathtt{B},\mathtt{B}} \mathbf{f}_{\mathtt{B}}^{(k+1)} = -\left[L(f^{(k)})\right]_{\mathtt{B},\mathtt{I}} \operatorname{diag}\left(\left|\mathbf{f}_{\mathtt{I}}^{(k)}\right|\right)^{-2} \mathbf{f}_{\mathtt{I}}^{(k)}.$$

Remark 3 Note that it is expected that the updated mapping would always have a smaller value of the stretch energy. Once the stretch energy $E_S(f^{(k+1)})$ is larger than $E_S(f^{(k)})$, we should stop the iteration and accept $f^{(k)}$ as the output.

The SEM algorithm for equiareal parameterizations is summarized in Algorithm 1.

6 Existence of Nontrivial Limit Points

In this section, we aim to prove the existence of a nontrivial (nonconstant) limit point of iterations of the SEM algorithm. For convenience, we give a mild assumption for the triangular mesh.

Definition 1 (Well-conditioned mesh) A simply connected open mesh $\mathcal{M}$ is said to be *well-conditioned* if it satisfies the following conditions:

(i) The subgraph of all the interior vertices is connected.
(ii) Every boundary vertex is connected to at least one interior vertex.

Also, we give the definition of M-matrix [7] and some related lemmas.

Definition 2 (i) A matrix $A \in \mathbb{R}^{m \times n}$ is said to be nonnegative (positive) if all the entries of A are nonnegative (positive).

Algorithm 1 Stretch Energy Minimization (SEM)

Input: A mesh $\mathcal{M}$ of a simply connected open surface.
Output: An equiareal parameterization f.

Compute the mesh area $\mathcal{A}(\mathcal{M}) := \sum_{\tau\in\mathcal{F}(\mathcal{M})} |\tau|$.
Compute the initial boundary mapping $\mathbf{f}_{\mathtt{B}}$ by $\mathbf{f}_{\mathtt{B}(j)} = \cos\theta_j + \mathrm{i}\sin\theta_j$,
in which $\theta_j = 2\pi(\sum_{\ell=1}^{j} |v_{\mathtt{B}(\ell+1)} - v_{\mathtt{B}(\ell)}|)/(\sum_{\ell=1}^{n_{\mathtt{B}}} |v_{\mathtt{B}(\ell+1)} - v_{\mathtt{B}(\ell)}|)$,
for $j = 1, \ldots, n_{\mathtt{B}}$, $v_{\mathtt{B}(n_{\mathtt{B}}+1)} := v_{\mathtt{B}(1)}$.
Compute the initial interior mapping by solving $L_{\mathtt{I},\mathtt{I}}\mathbf{f}_{\mathtt{I}} = -L_{\mathtt{I},\mathtt{B}}\mathbf{f}_{\mathtt{B}}$.
Update the Laplacian matrix: $L \leftarrow L(f)$.
while not convergent **do**
  Store the current mapping: $g = f$.
  Update the boundary by solving $L_{\mathtt{B},\mathtt{B}}\mathbf{f}_{\mathtt{B}} = -L_{\mathtt{B},\mathtt{I}}\mathbf{f}_{\mathtt{I}}$.
  Centralize the boundary: $\mathbf{f}_{\mathtt{B}} \leftarrow \left(I_{n_{\mathtt{B}}} - \frac{\mathbf{1}_{n_{\mathtt{B}}}\mathbf{1}_{n_{\mathtt{B}}}^{\top}}{n_{\mathtt{B}}}\right)\mathbf{f}_{\mathtt{B}}$.
  Normalize the boundary: $\mathbf{f}_{\mathtt{B}} \leftarrow \mathrm{diag}\left(|\mathbf{f}_{\mathtt{B}}|^{-1}\right)\mathbf{f}_{\mathtt{B}}$.
  Update the interior by solving $L_{\mathtt{I},\mathtt{I}}\mathbf{f}_{\mathtt{I}} = -L_{\mathtt{I},\mathtt{B}}\mathbf{f}_{\mathtt{B}}$.
  if $E_S(f) > E_S(g)$ **then**
    Adopt the previous mapping: $f = g$.
    break
  end if
  Update the Laplacian matrix: $L \leftarrow L(f)$.
end while

(ii) A squared matrix $A \in \mathbb{R}^{n\times n}$ is irreducible, if the corresponding graph $\mathcal{G}(A)$ of A is connected.

Definition 3 A matrix $A \in \mathbb{R}^{n\times n}$ is said to be an M-matrix if $A = sI - B$, where B is nonnegative and $s \geq \rho(B)$, where $\rho(B)$ is the spectral radius of B.

Lemma 1 (Theorem 1.4.10 in [21]) *Suppose $A \in \mathbb{R}^{n\times n}$ is a singular, irreducible M-matrix. Then each principal submatrix of A other than A itself is a nonsingular M-matrix.*

Lemma 2 (Theorem 1.4.7 in [21]) *If $A \in \mathbb{R}^{n\times n}$ is a nonsingular M-matrix, then A^{-1} is a nonnegative matrix. Moreover, if A is irreducible, then A^{-1} is a positive matrix.*

Lemma 3 (Perron Theorem [17]) *Let $A \in \mathbb{R}^{n\times n}$ be a positive matrix. Then*

(i) $\rho(A)$ is an eigenvalue of A, and all the other eigenvalues are strictly smaller than $\rho(A)$ in modulus.
(ii) $\rho(A)$ is the only eigenvalue that has a positive eigenvector.
(iii) $\rho(A)$ has algebraic multiplicity one.

The following theorem plays an important role in the geometric point of view of the matrix product of $K^{(k)}$ in Eq. (23).

Theorem 2 *Given a well-conditioned simply connected open mesh $\mathcal{M}$ with n vertices. Let $L^{(1)}$ and $L^{(2)}$ be two Laplacian matrices of $\mathcal{M}$, defined similar as in (6), with positive weights $\{w_{i,j}^{(1)} \,|\, [v_i, v_j] \in \mathcal{E}(\mathcal{M})\}$ and $\{w_{i,j}^{(2)} \,|\, [v_i, v_j] \in \mathcal{E}(\mathcal{M})\}$, respectively. Let $\mathtt{I}$ and $\mathtt{B}$ be index sets of interior vertices and boundary vertices, respectively. Let*

$$K = \left[L_{\mathtt{B},\mathtt{B}}^{(2)}\right]^{-1}\left[L_{\mathtt{I},\mathtt{B}}^{(2)}\right]^{\top}\left[L_{\mathtt{I},\mathtt{I}}^{(1)}\right]^{-1}L_{\mathtt{I},\mathtt{B}}^{(1)}.$$

Then K is positive with $\rho(K) = 1$ being the unique largest eigenvalue of K in modulus.

Proof From the definition of the Laplacian matrix (6), it is clear that $L^{(t)}\mathbf{1}_{n_L} = \mathbf{0}$, for $t = 1, 2$, i.e.,

$$\begin{cases} L^{(t)}_{\mathtt{I},\mathtt{I}}\mathbf{1}_{n_{\mathtt{I}}} + L^{(t)}_{\mathtt{I},\mathtt{B}}\mathbf{1}_{n_{\mathtt{B}}} = \mathbf{0}, \\ \left[L^{(t)}_{\mathtt{I},\mathtt{B}}\right]^{\top}\mathbf{1}_{n_{\mathtt{I}}} + L^{(t)}_{\mathtt{B},\mathtt{B}}\mathbf{1}_{n_{\mathtt{B}}} = \mathbf{0}. \end{cases} \tag{24}$$

Note that $L^{(t)}$ is a singular irreducible M-matrix, for $t = 1, 2$. By Lemma 1, the matrices $L^{(t)}_{\mathtt{I},\mathtt{I}}$ and $L^{(t)}_{\mathtt{B},\mathtt{B}}$ are invertible. Then Eq. (24) implies that

$$\begin{cases} \left[L^{(t)}_{\mathtt{I},\mathtt{I}}\right]^{-1} L^{(t)}_{\mathtt{I},\mathtt{B}}\mathbf{1}_{n_{\mathtt{B}}} = -\mathbf{1}_{n_{\mathtt{I}}}, \\ \left[L^{(t)}_{\mathtt{B},\mathtt{B}}\right]^{-1}\left[L^{(t)}_{\mathtt{I},\mathtt{B}}\right]^{\top}\mathbf{1}_{n_{\mathtt{I}}} = -\mathbf{1}_{n_{\mathtt{B}}}. \end{cases} \tag{25}$$

It follows from Eq. (25) that

$$\begin{aligned} K\mathbf{1}_{n_{\mathtt{B}}} &= \left[L^{(2)}_{\mathtt{B},\mathtt{B}}\right]^{-1}\left[L^{(2)}_{\mathtt{I},\mathtt{B}}\right]^{\top}\left[L^{(1)}_{\mathtt{I},\mathtt{I}}\right]^{-1} L^{(1)}_{\mathtt{I},\mathtt{B}}\mathbf{1}_{n_{\mathtt{B}}} \\ &= -\left[L^{(2)}_{\mathtt{B},\mathtt{B}}\right]^{-1}\left[L^{(2)}_{\mathtt{I},\mathtt{B}}\right]^{\top}\mathbf{1}_{n_{\mathtt{I}}} = \mathbf{1}_{n_{\mathtt{B}}}. \end{aligned} \tag{26}$$

That is, 1 is an eigenvalue of K associated with the eigenvector $\mathbf{1}_{n_{\mathtt{B}}}$. On the other hand, the irreducibilities of $L^{(1)}_{\mathtt{I},\mathtt{I}}$ and $L^{(2)}_{\mathtt{B},\mathtt{B}}$ are respectively guaranteed by Definition 1 (i) and the assumption that $\mathcal{M}$ has only one boundary. By Lemma 2, $[L^{(1)}_{\mathtt{I},\mathtt{I}}]^{-1}$ and $[L^{(2)}_{\mathtt{B},\mathtt{B}}]^{-1}$ are positive. Furthermore, Definition 1 (ii) and the positivity of $[L^{(1)}_{\mathtt{I},\mathtt{I}}]^{-1}$ guarantee that $[L^{(2)}_{\mathtt{I},\mathtt{B}}]^{\top}[L^{(1)}_{\mathtt{I},\mathtt{I}}]^{-1}L^{(1)}_{\mathtt{I},\mathtt{B}}$ is positive. Then the positivity of K is guaranteed by the positivity of $[L^{(2)}_{\mathtt{B},\mathtt{B}}]^{-1}$. Hence, By Lemma 3, $\rho(K) = 1$ is the largest eigenvalue of K with algebraic multiplicity one, and all the other eigenvalues are strictly smaller than 1 in modulus. □

Remark 4 In general, if some weights of the stretched Laplacian matrix (14) are negative, the flip algorithm [8] is recommended to achieve positive weights.

In the following, we prove the existence of limit points of the iterative scheme (23).

Theorem 3 *Suppose the sequence $\{\mathbf{f}^{(k)}_{\mathtt{B}}\}_{k\in\mathbb{N}}$ defined in (23) with $K^{(k)}$ satisfying the assumption of Theorem 2. Then it has a limit point $\mathbf{f}^{(*)}_{\mathtt{B}} \neq \mathbf{1}_{n_{\mathtt{B}}}$.*

Proof Since every entry of $\mathbf{f}^{(k)}_{\mathtt{B}}$ is on the unit circle, by Bolzano-Weierstrass theorem there exists a vector $\mathbf{f}^{(*)}_{\mathtt{B}}$ and a convergent subsequence $\{\mathbf{f}^{(k_j)}_{\mathtt{B}}\}_{j\in\mathbb{N}}$ such that

$$\lim_{j\to\infty}\mathbf{f}^{(k_j)}_{\mathtt{B}} = \mathbf{f}^{(*)}_{\mathtt{B}}.$$

From (26) of Theorem 2, geometrically, for $i = 1, \ldots, n_{K^{(k)}}$, $(K^{(k)}\mathbf{f})_i = \sum_{j=1}^{n_{K^{(k)}}} K^{(k)}_{i,j}\mathbf{f}_j$ is a strictly convex combination of the points $\mathbf{f}_j \in \mathbb{C}$, $j = 1, \ldots, n_{K^{(k)}}$. As a result,

the centralization in the iteration (23) guarantees that after a rotation by setting $\mathbf{f}_{\mathtt{B}(1)}^{(k)} = 1$ for each $k \in \mathbb{N}$, the maximal argument satisfies

$$\max_{1\le \ell \le n_{\mathtt{B}}} \operatorname{Arg}\left((CK^{(k)}\mathbf{f}_{\mathtt{B}}^{(k)})_\ell\right) > \pi. \tag{27}$$

Otherwise, each entry of the vector $CK^{(k)}\mathbf{f}_{\mathtt{B}}^{(k)}$ is located on the upper half-plane of $\mathbb{C}$. Then the center

$$\frac{1}{n_{\mathtt{B}}}\sum_{i=1}^{n_{\mathtt{B}}}(CK^{(k)}\mathbf{f}_{\mathtt{B}}^{(k)})_i \neq 0,$$

which contradicts that the center should be zero. In particular, Eq. (27) holds for the subsequence $\{k_j\}_{j\in\mathbb{N}}$. Hence, the accumulation point $\mathbf{f}_{\mathtt{B}}^{(*)}$ satisfies

$$\max_{1\le \ell \le n_{\mathtt{B}}} \operatorname{Arg}\left((CK^{(k)}\mathbf{f}_{\mathtt{B}}^{(*)})_\ell\right) \ge \pi.$$

Therefore, $\mathbf{f}_{\mathtt{B}}^{(*)} \neq \mathbf{1}_{n_{\mathtt{B}}}$. □

7 Numerical Experiments

In this section, we demonstrate numerical results of equiareal parameterizations obtained by the SEM algorithm. Comparisons of the SEM algorithm and the other state-of-the-art algorithms in terms of effectiveness and accuracy are demonstrated thereafter. The maximal numbers of iterations for the SEM algorithm are set to be 10. The linear systems in the SEM algorithm are solved using the backslash operator (\) in MATLAB. Some of mesh models are obtained from TurboSquid [5], AIM@SHAPE shape repository [3], the Stanford 3D scanning repository [4], and a project page of ALICE [1]. Each model in our experiments is a simply connected open mesh without *leaf-like structures* defined as follows.

Definition 4 (Leaf-like structure of triangular mesh) The set of vertices $\{v_i, v_j, v_k\}$ on a triangular mesh $\mathcal{M}$ is called a *leaf-like structure* if v_i, v_j, v_k are boundary vertices and $\{[v_i, v_j], [v_j, v_k], [v_k, v_i]\} \subset \mathcal{E}(\mathcal{M})$.

7.1 Equiareal Parameterizations by the SEM Algorithm

Fig. 2 shows mesh models of human faces of different facial expressions and some of benchmark mesh models, and their equiareal parameterizations computed by the SEM algorithm.

To measure the equiareal distortion, the *total area distortion* as well as the mean and the standard deviation (SD) of *local area ratios* for the parameterization are commonly used. The total area distortion (per vertex) of a mapping f on a mesh $\mathcal{M}$ is defined as

$$\mathcal{D}_{\mathcal{M}}(f) = \frac{1}{3}\sum_{v\in\mathcal{V}(\mathcal{M})}\left|\frac{\sum_{\tau\in\mathcal{N}(v)}|\tau|}{|\mathcal{M}|} - \frac{\sum_{\tau\in\mathcal{N}(v)}|f(\tau)|}{|f(\mathcal{M})|}\right|, \tag{28}$$

(a) *Liu Neutral* (b) *Liu Smiling*

(c) *Liu Wry* (d) *Liu Pouting*

(e) *Stanford Bunny* (f) *Human Brain*

(g) *Chinese Lion* (h) *Left Hand*

Fig. 2 The mesh models of human faces of different facial expressions and some of benchmark mesh models, and their equiareal parameterizations computed by the SEM algorithm.

where $\mathcal{N}(v) = \{\tau \in \mathcal{F}(\mathcal{M}) \,|\, v \subset \tau\}$ is the set of neighboring faces of the vertex v, $|\mathcal{M}|$ and $|f(\mathcal{M})|$ denote areas of $\mathcal{M}$ and its image, respectively. A mapping f, defined on $\mathcal{M}$, is area-preserving if $\mathcal{D}_{\mathcal{M}}(f) = 0$. The local area ratio $\mathcal{R}_f$ on a vertex v is defined as

$$\mathcal{R}_f(v) = \frac{\sum_{\tau \in \mathcal{N}(v)} |\tau| / |\mathcal{M}|}{\sum_{\tau \in \mathcal{N}(v)} |f(\tau)| / |f(\mathcal{M})|}. \tag{29}$$

The mean and the SD of $\mathcal{R}_f(v)$, for all $v \in \mathcal{V}(\mathcal{M})$, are used to measure the local area distortion. A mapping f is area-preserving if the mean is 1 and the SD is 0.

Note that the idealized local area ratio is 1. Fig. 3 shows distributions of differences between 1 and local area ratios of equiareal parameterizations obtained by the SEM algorithm for mesh models of human faces and some of benchmarks. Fig. 4 further shows histograms of local area ratios, which indicate that local area ratios of most triangular faces are close to 1, as we desired.

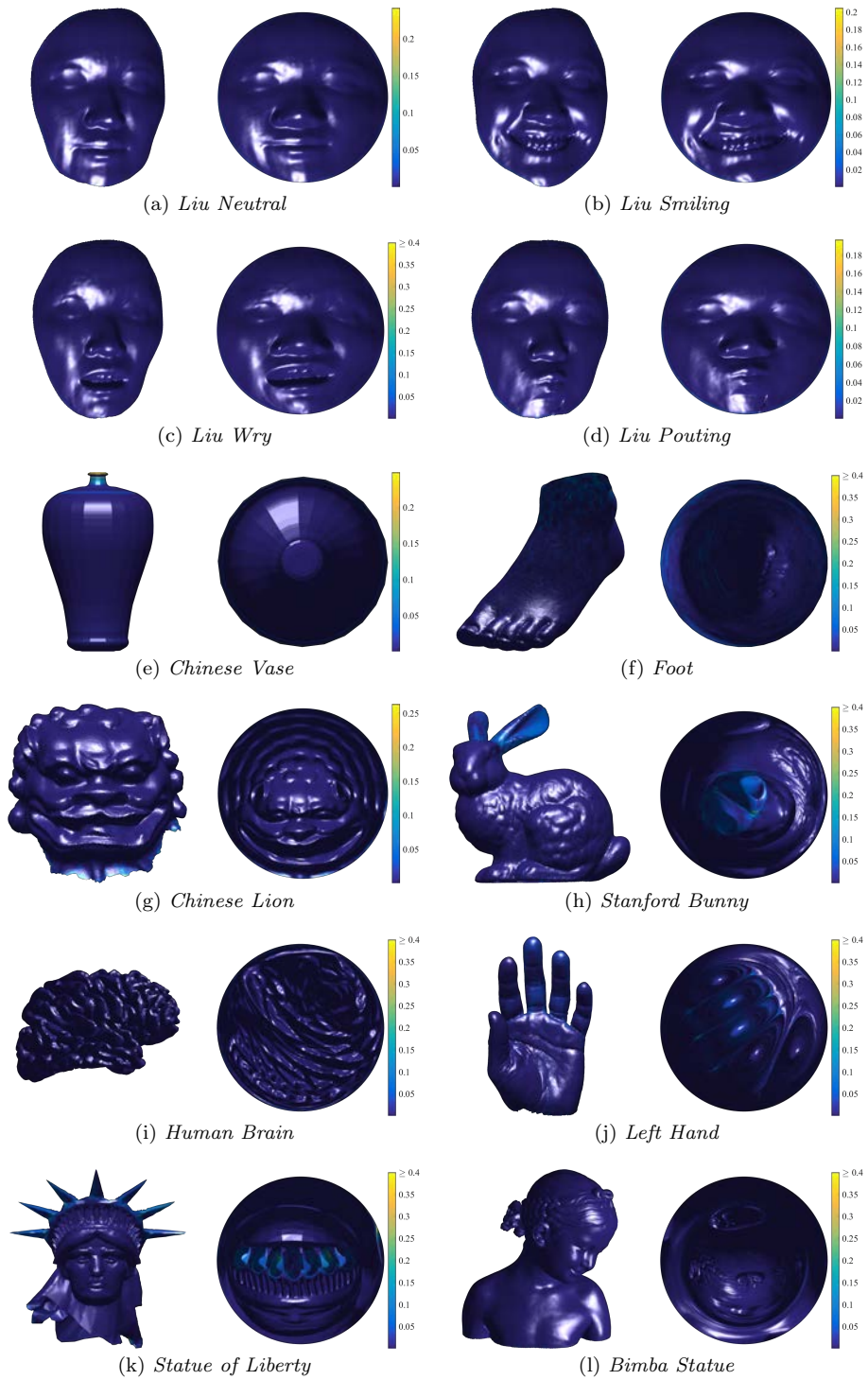

(a) *Liu Neutral* (b) *Liu Smiling*

(c) *Liu Wry* (d) *Liu Pouting*

(e) *Chinese Vase* (f) *Foot*

(g) *Chinese Lion* (h) *Stanford Bunny*

(i) *Human Brain* (j) *Left Hand*

(k) *Statue of Liberty* (l) *Bimba Statue*

Fig. 3 Distributions of differences between 1 and local area ratios of equiareal parameterizations obtained by the SEM algorithm.

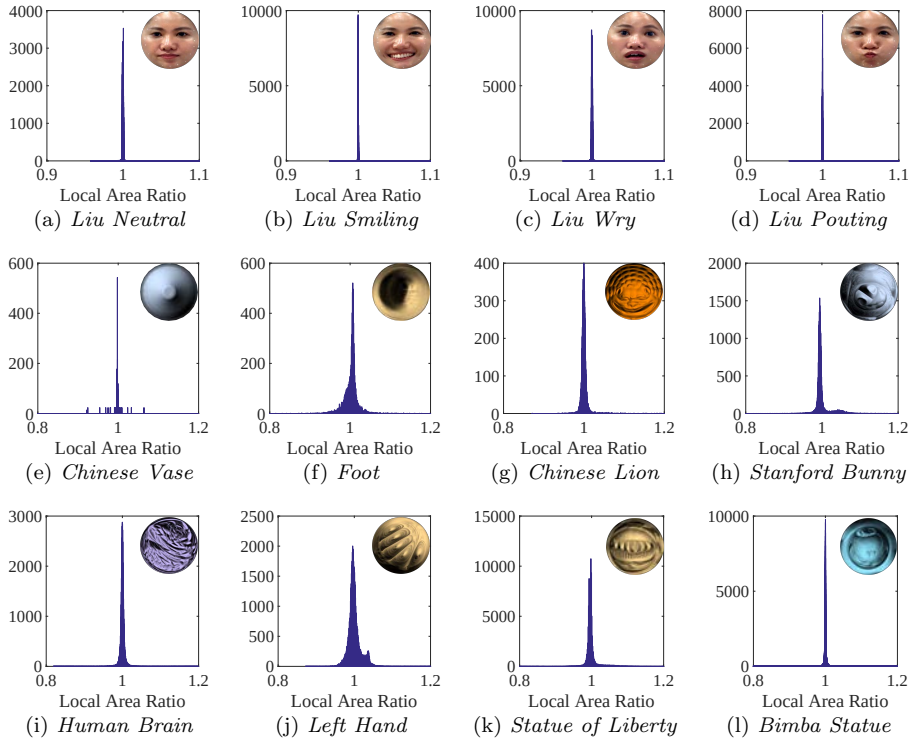

Fig. 4 Histograms of local area ratios $\mathcal{R}_f(v)$ in (29) of equiareal parameterizations obtained by the SEM algorithm.

Fig. 5 shows distributions of angular distortions of equiareal parameterizations by the SEM algorithm for mesh models of human faces and some of benchmarks. The angular distortion refers to the absolute value of the difference (counted in degree) between the angle on the mesh model and the disk. Fig. 6 further shows histograms of angular distortions. As shown in Fig. 6 (a)–(d), most of angular distortions are less than 30 degrees, which is acceptable. Note that the geometry of human faces is simple, so the mapping by the SEM algorithm would not produce large angular distortions significantly. However, when the geometry of the surface is much more complicated, e.g., the model of *Left Hand* shown in Fig. 2 (h), large angular distortions might appear. As shown in Fig. 6 (j), lots of angles have distortions larger than 50 degrees.

On the other hand, Fig. 7 shows the relationship between the number of iterations and the total area distortion as well as the stretch energy. These results indicate that the total area distortion decreases while the stretch energy is decreasing. In other words, it is reasonable to compute an equiareal parameterization via minimizing the stretch energy. In addition, as shown in Fig. 7, both the total area distortion and the stretch energy are significantly decreased in the first three iteration steps, which shows the effectiveness of the proposed SEM algorithm.

Fig. 8 further shows the first 5 iteration steps of the SEM algorithm for computing the equiareal parameterization of the mesh model *Nefertiti*. The color indicates the absolute value of the difference between the local area ratio and 1. In Fig. 8,

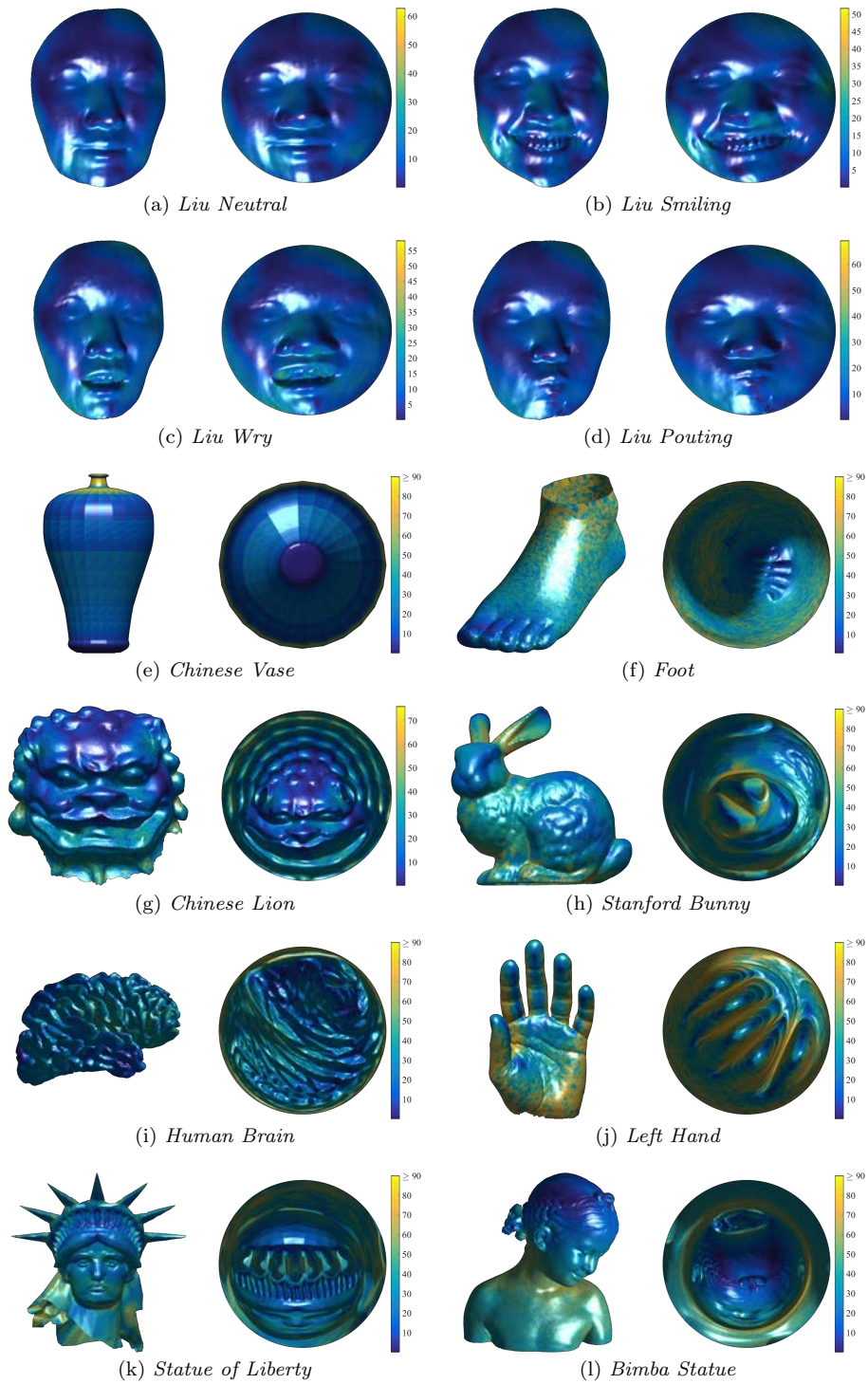

(a) *Liu Neutral* (b) *Liu Smiling*

(c) *Liu Wry* (d) *Liu Pouting*

(e) *Chinese Vase* (f) *Foot*

(g) *Chinese Lion* (h) *Stanford Bunny*

(i) *Human Brain* (j) *Left Hand*

(k) *Statue of Liberty* (l) *Bimba Statue*

Fig. 5 The distributions of the angular distortion of the equiareal parameterizations obtained by the SEM algorithm. The angular distortion refers to the absolute value of the difference (counted in degree) between the angle on the mesh model and the disk.

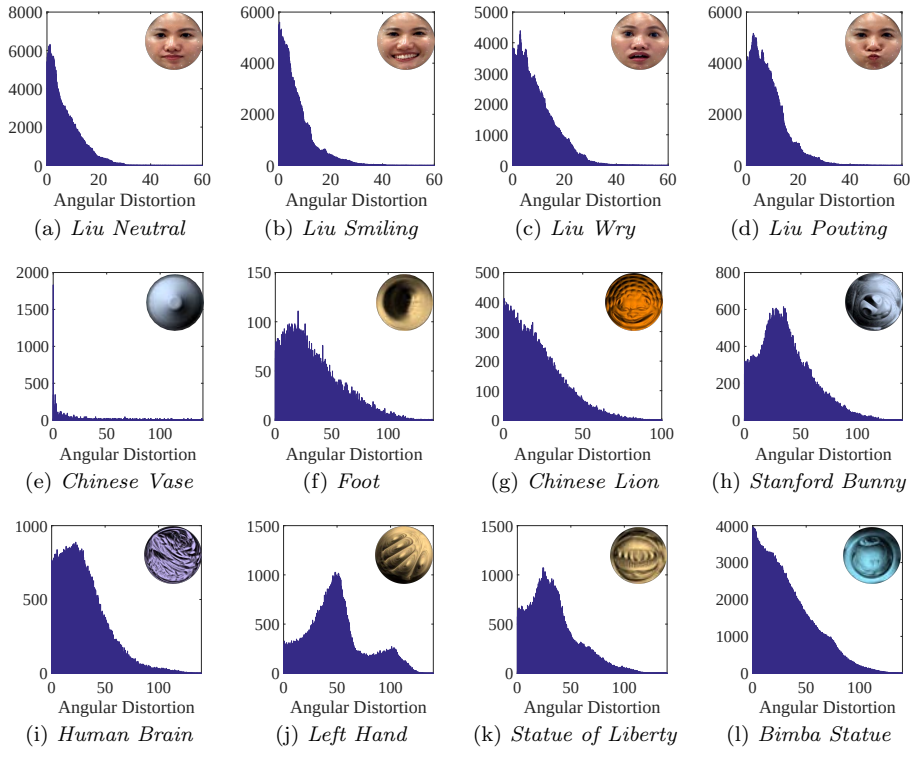

Fig. 6 The histograms of angular distortions of the equiareal parameterizations obtained by the SEM algorithm. The angular distortion refers to the absolute value of the difference (counted in degree) between the angle on the mesh model and the disk.

we observe that the local area distortion of the initial harmonic mapping is dominant at the nose region. However, the distortion is significantly decreased after 1 iteration step. This indicates that the proposed SEM algorithm works well on decreasing the local area distortion.

7.2 Comparisons with State-of-the-Art Algorithms

We now compare equiareal parameterizations computed by the proposed SEM algorithm with that of the other state-of-the-art algorithms in terms of effectiveness and accuracy, respectively.

Although the Lie advection method [31] based on Lie derivative and Cartans formula can handle surfaces with complicated topologies, however, the iterative procedure for optimizing triangulations in [31] is indirect and less efficient [25]. Therefore, we compare the effectiveness and the accuracy of our SEM algorithm to two of the state-of-the-art algorithms of equiareal parameterizations for simply connected open surfaces, namely, the fast stretch minimization (FSM) algorithm [27] and the optimal mass transportation (OMT) algorithm [25]. The MATLAB code of the FSM algorithm is reproduced by authors. The executable program files of the OMT algorithm are obtained from Gu's website [2].

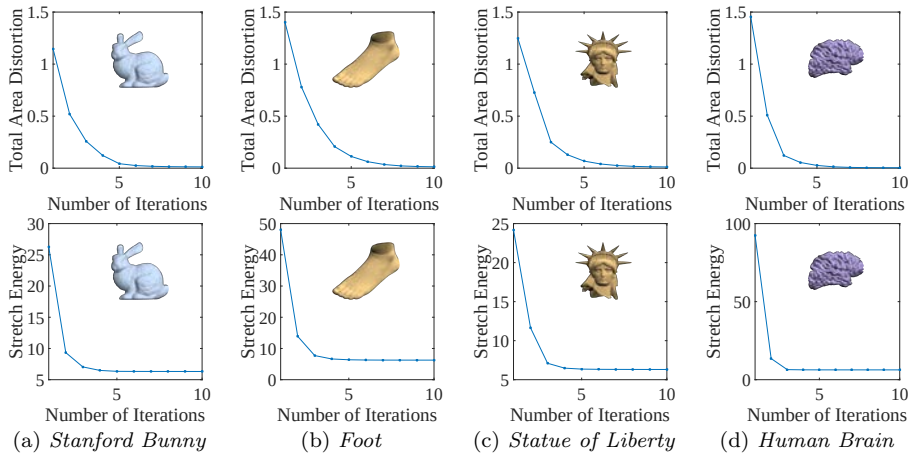

(a) *Stanford Bunny* (b) *Foot* (c) *Statue of Liberty* (d) *Human Brain*

Fig. 7 The relationship between the number of iterations and the total area distortion as well as the stretch energy of the parameterization obtained by the SEM algorithm for (a) *Stanford Bunny*, (b) *Foot*, (c) *Statue of Liberty* and (d) *Human Brain*.

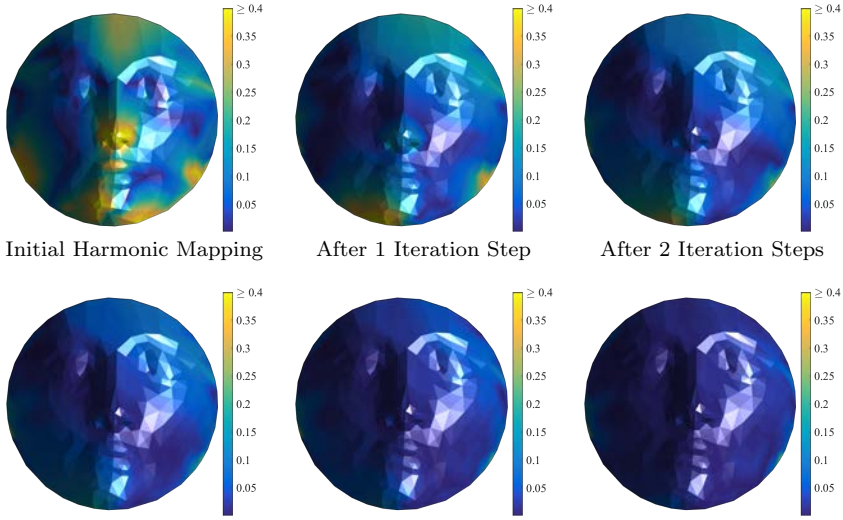

Initial Harmonic Mapping | After 1 Iteration Step | After 2 Iteration Steps

After 3 Iteration Steps | After 4 Iteration Steps | After 5 Iteration Steps

Fig. 8 The first 5 iteration steps of the SEM algorithm for *Nefertiti*. The color indicates the absolute value of the difference between the local area ratio and 1.

A comparison of the computational cost between FSM, OMT and the SEM algorithms is demonstrated in Table 1. The notation "−" means the iteration of algorithms does not converge. Also, Fig. 9 illustrates the relationship between the number of triangular faces and the computational cost. As shown in Fig. 9 (a), the effectiveness of the SEM outperforms the OMT, especially when the number of faces is large. In addition, in Fig. 9 (b), the computational cost of FSM is roughly double of the cost of the SEM algorithm. These results are consistent with the

Table 1 The computational cost (sec.) of equiareal parameterizations by FSM [27], OMT [25], and the SEM algorithms. The notation "−" means the iteration of algorithms does not converge.

Model Name	# Faces	FSM [27]		OMT [25]		SEM	
		Time	#Iter.	Time	#Iter.	Time	#Iter.
Nefertiti	562	0.10	10	0.12	26	0.10	10
Cowboy Hat	4,604	0.14	10	1.37	68	0.08	10
Chinese Vase	5,592	0.14	10	–	–	0.07	10
Bourbon Bottle	13,088	–	–	–	–	0.23	10
Foot	19,966	–	–	7.11	104	0.36	10
Chinese Lion	34,421	1.24	10	4.29	26	0.69	10
Stanford Bunny	65,221	–	–	–	–	1.76	10
Human Brain	96,811	–	–	30.89	58	2.58	10
Left Hand	105,860	–	–	–	–	2.65	10
Statue of Liberty	190,156	–	–	–	–	4.49	10
Liu Neutral	193,298	9.63	10	28.15	20	5.38	10
Liu Smiling	205,207	10.22	10	30.56	20	5.65	10
Liu Pouting	207,721	10.37	10	30.89	20	5.81	10
Liu Wry	208,283	10.39	10	30.68	20	5.87	10
Isis Statue	374,306	–	–	–	–	12.18	10
Bimba Statue	836,734	–	–	854.06	124	28.16	10
Knit Cap Man	1,287,579	–	–	1753.11	66	70.23	10

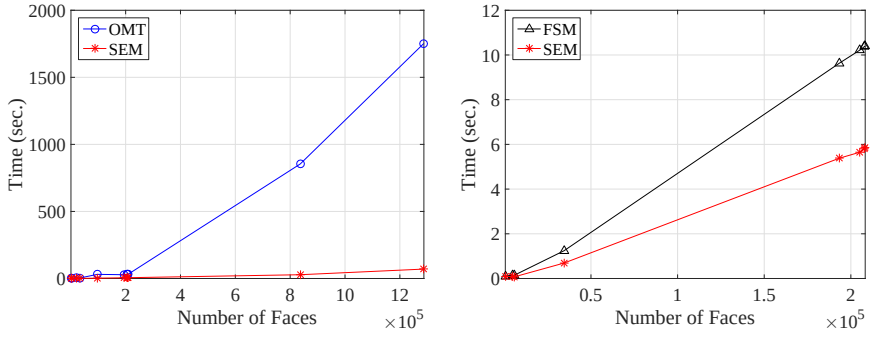

(a) OMT vs SEM (b) FSM vs SEM

Fig. 9 Computational cost (sec.) versus number of faces by FSM, OMT, and the SEM.

fact that the LU decomposition requires roughly $\frac{2}{3}n^3$ floating-point operations (FLOPs) while the Cholesky decomposition only requires $\frac{1}{3}n^3$ FLOPs.

Comparisons of the total area distortion (28) as well as the mean and the SD of local area ratios (29) for equiareal parameterizations are demonstrated in Table 2 and Fig. 10 as well as Table 3 and Fig. 11, respectively. As shown in Fig. 10, among three algorithms, the total area distortion produced by the SEM algorithm is always the smallest and less than 2%, which is satisfactory in practical applications. Similarly, Fig. 11 indicates that the SEM algorithm has a better accuracy of the mean and the SD of local area ratios than that of FSM and OMT. In addition, for every demonstrated mesh model, the iteration of the SEM algorithm converges, while, for some mesh models, the iteration of FSM or OMT does not converge. It is fairly said that the proposed SEM algorithm is much more robust.

Table 2 The total area distortion $\mathcal{D}_{\mathcal{M}}(f)$ in (28) of equiareal parameterizations computed by FSM, OMT, and the SEM algorithms. The notation "−" means the iteration of algorithms does not converge.

Model Name	# Faces	FSM [27]	OMT [25]	SEM
Nefertiti	562	0.1199	0.0804	0.0092
Cowboy Hat	4,604	0.0704	0.1000	0.0015
Chinese Vase	5,592	0.5188	–	0.0036
Bourbon Bottle	13,088	–	–	0.0115
Foot	19,966	–	0.1330	0.0136
Chinese Lion	34,421	0.2102	0.0793	0.0036
Stanford Bunny	65,221	–	–	0.0124
Human Brain	96,811	–	0.0765	0.0041
Left Hand	105,860	–	–	0.0116
Statue of Liberty	190,156	–	–	0.0117
Liu Neutral	193,298	0.0338	0.0364	0.0012
Liu Smiling	205,207	0.0345	0.0370	0.0010
Liu Pouting	207,721	0.0406	0.0368	0.0010
Liu Wry	208,283	0.0618	0.0381	0.0013
Isis Statue	374,306	–	–	0.0062
Bimba Statue	836,734	–	0.0873	0.0020
Knit Cap Man	1,287,579	–	0.1089	0.0046

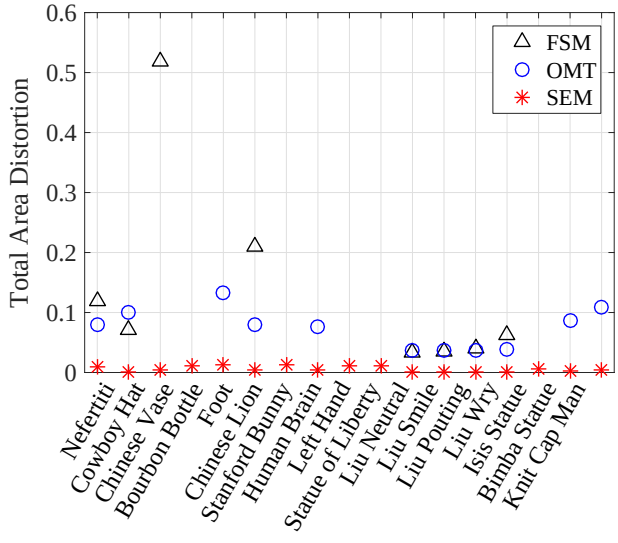

Fig. 10 The total area distortion of the equiareal parameterizations computed by FSM, OMT, and the SEM algorithms.

8 Applications

In this section, we demonstrate some sample applications of the proposed SEM algorithm, namely, surface remeshing in Sect. 8.1, surface registration in Sect. 8.2 and surface morphing in Sect. 8.3.

Table 3 The mean and SD of local area ratios $\mathcal{R}_f(v)$ in (29) of equiareal parameterizations by FSM [27], OMT [25] and the SEM algorithms. The notation "−" means the iteration of algorithms does not converge.

Model Name	# Faces	FSM [27]		OMT [25]		SEM	
		Mean	SD	Mean	SD	Mean	SD
Nefertiti	562	1.0359	0.1222	0.9962	0.1208	1.0038	0.0465
Cowboy Hat	4,604	1.0447	0.0820	1.0122	0.1887	0.9999	0.0020
Chinese Vase	5,592	1.0766	0.9141	–	–	0.9992	0.0399
Bourbon Bottle	13,088	–	–	–	–	0.9989	0.0528
Foot	19,966	–	–	0.9939	0.1686	1.0022	0.0227
Chinese Lion	34,421	1.0566	0.2290	0.9976	0.1054	1.0003	0.0103
Stanford Bunny	65,221	–	–	–	–	1.0004	0.0251
Human Brain	96,811	–	–	1.0016	0.1112	1.0003	0.0125
Left Hand	105,860	–	–	–	–	1.0005	0.0214
Statue of Liberty	190,156	–	–	–	–	1.0013	0.0541
Liu Neutral	193,298	1.0021	0.0505	1.0021	0.0516	1.0003	0.0078
Liu Smiling	205,207	1.0028	0.0509	1.0024	0.0505	1.0003	0.0080
Liu Pouting	207,721	1.0033	0.0575	1.0026	0.0514	1.0004	0.0083
Liu Wry	208,283	1.0090	0.0759	1.0022	0.0520	1.0004	0.0087
Isis Statue	374,306	–	–	–	–	1.0001	0.0145
Bimba Statue	836,734	–	–	0.9945	0.1392	1.0002	0.0086
Knit Cap Man	1,287,579	–	–	1.0076	0.1413	1.0013	0.0225

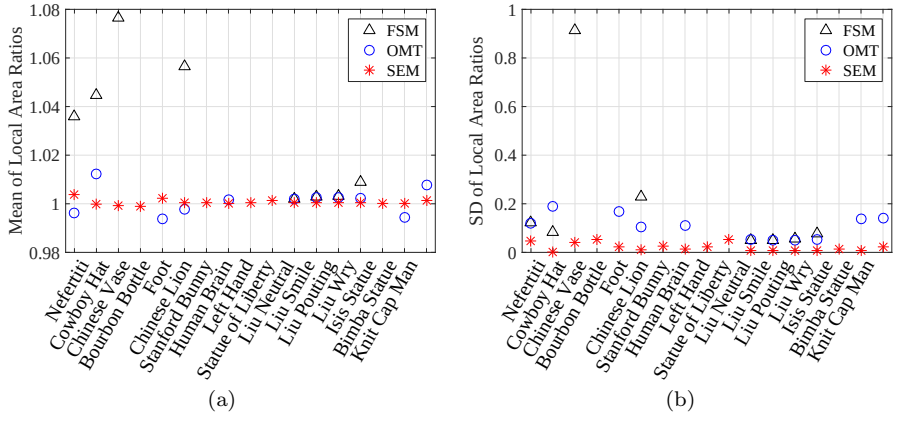

Fig. 11 The (a) mean and (b) standard deviation of local area ratios of parameterizations by FSM, OMT and the SEM algorithms.

8.1 Surface Remeshing for Human Face Models

Surface remeshing refers as to the improvement process of the mesh quality in terms of vertex sampling, regularity and triangle quality [6,9]. In numerical experiments, the raw mesh data of human faces are captured by the structured-light 3D scanner *GeoVideo* (GI company) in the ST Yau Center of Chiao Tung Univ., Taiwan. For example, in the raw mesh data of a human face $\mathcal{M}$, shown in Fig. 12 (a), the areas of triangles are very different. The equiareal parameterization can be applied to the surface remeshing so that the vertex sampling on $\mathcal{M}$ becomes uniform and the mesh becomes regular after the remeshing process.

The remeshing procedure is described as follows. First, a bijective equiareal mapping $f : \mathcal{M} \to \mathbb{D} \subset \mathbb{C}$ is computed by using the SEM algorithm. Then the im-

age $f(\mathcal{M})$ is covered by a regular mesh $\mathcal{U}$ of a unit disk with a uniform sampling. Finally, the remeshed surface $f^{-1}(\mathcal{U})$ is obtained by the one-to-one correspondences between the barycentric coordinates of $\mathcal{M}$ and $f(\mathcal{M})$.

Fig. 12 shows the zoom-in images at the nose part and the histograms of the areas of triangles of the raw mesh data and the remeshed data of the human face, respectively, which indicate that the sampling of vertices becomes more uniform after the remeshing process. In addition, some obtuse triangles at the nose part disappear after the process. From Fig. 6 (a)–(d), we observe that the angular distortions of the equiareal parameterizations of human faces by the SEM algorithm are not large so that the remeshed data of human faces look so satisfactory.

In general, the described remeshing procedure using the equiareal parameterization could only guarantee that the sampling of the vertices in the remeshed model would become uniform. Lots of obtuse triangles might appear when angular distortions of parameterizations are large. For example, the equiareal parameterization could be applied to obtain a uniform sampling of vertices for the *Left Hand* model, shown in Fig. 2 (d). However, the triangle quality of the remeshed data by the described remeshing procedure would not be satisfactory.

8.2 Surface Registration

The surface registration is a fundamental problem that has been widely applied to geometry processing tasks [18, 20, 26]. Given two simply connected open meshes $\mathcal{M}$ and $\mathcal{N}$ with m and n vertices, respectively, and a set of landmark pairs

$$\{(p_\ell, q_\ell) \,|\, p_\ell \in \mathcal{M}, q_\ell \in \mathcal{N}\}_{\ell=1}^{d}.$$

The goal of the surface registration is to construct a smooth bijective mapping $\phi : \mathcal{M} \to \mathcal{N}$ such that $\phi(p_\ell) = q_\ell$. With the help of the parameterization mappings

$$f : \mathcal{M} \to \mathbb{D} \quad \text{and} \quad g : \mathcal{N} \to \mathbb{D}, \tag{30}$$

the surface registration problem in the three-dimensional space is reduced into a planar registration problem on a unit disk. Recall that $f : \mathcal{M} \to \mathbb{D}$ and $g : \mathcal{N} \to \mathbb{D}$ in (30) are the disk-shaped parameterizations of the surfaces $\mathcal{M}$ and $\mathcal{N}$, respectively, which can be computed efficiently by the conformal energy minimization (CEM) algorithm [29]. Then the reduced problem is to find a smooth bijective mapping $h : \mathbb{D} \to \mathbb{D}$ such that

$$h \circ f(p_\ell) = g(q_\ell),$$

for $\ell = 1, \ldots, d$. Then the mapping $\varphi : \mathcal{M} \to \mathcal{N}$ is obtained by $\varphi := g^{-1} \circ h \circ f$. In this section, we propose an efficient algorithm for computing registration mappings on a unit disk. First, a boundary mapping is introduced in Sect. 8.2.1. Then a smooth registration mapping for the given boundary condition is proposed in Sect. 8.2.2. In order to deal with the registration mapping of large deformations, a generalized algorithm is developed in Sect. 8.2.3.

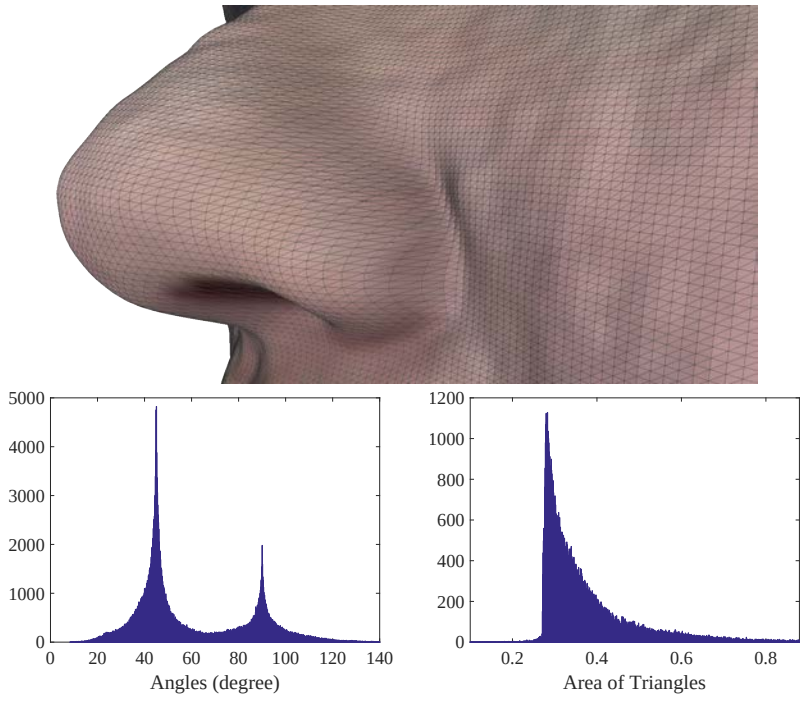

(a) The raw mesh data

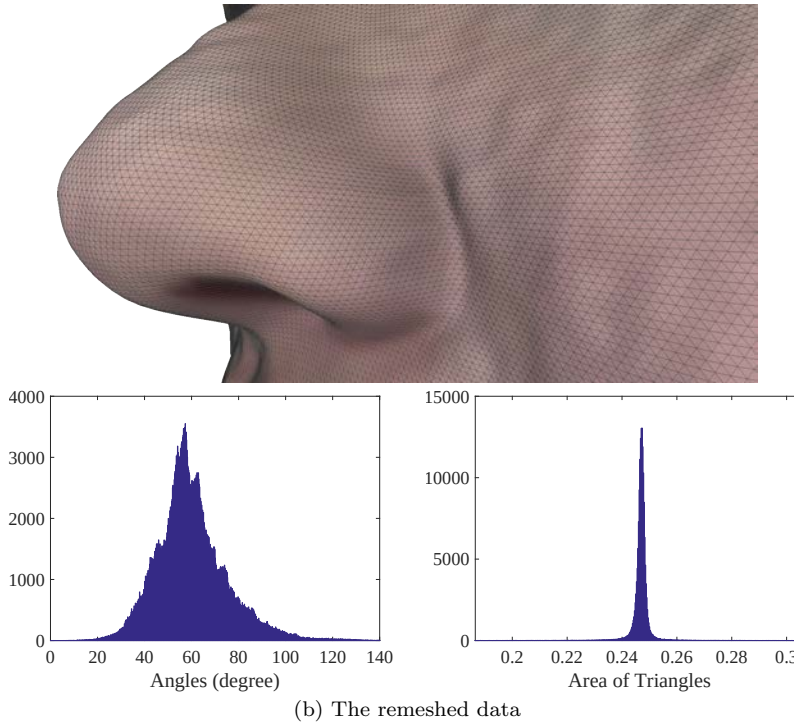

(b) The remeshed data

Fig. 12 The zoom-in images at the nose part and the histograms of the angles and areas of triangles of (a) the raw mesh data and (b) the remeshed data of a human face.

8.2.1 Boundary Registration Mapping

Without loss of generality, we assume that

$$\begin{cases} p_1, \ldots, p_c \in \mathcal{M} \backslash \partial\mathcal{M} \\ p_{c+1}, \ldots, p_d \in \partial\mathcal{M} \end{cases} \quad \text{and} \quad \begin{cases} q_1, \ldots, q_c \in \mathcal{N} \backslash \partial\mathcal{N} \\ q_{c+1}, \ldots, q_d \in \partial\mathcal{N} \end{cases},$$

respectively. Suppose the landmarks on the boundary are sorted counterclockwise and separate $\partial\mathcal{M}$ and $\partial\mathcal{N}$ into segments of curves

$$\gamma_{[p_d,p_{c+1}]}, \gamma_{[p_{c+1},p_{c+2}]}, \ldots, \gamma_{[p_{d-1},p_d]} \quad \text{and} \quad \gamma_{[q_d,q_{c+1}]}, \gamma_{[q_{c+1},q_{c+2}]}, \ldots, \gamma_{[q_{d-1},q_d]},$$

respectively. The conformal mappings can be modified by Möbius transformations Möb_f and Möb_g such that

$$\text{Möb}_f \circ f(p_\ell) = 0 \quad \text{and} \quad \text{Möb}_g \circ g(q_\ell) = 0,$$

for some ℓ, i.e.,

$$\text{Möb}_f \circ f(v_j) = \frac{f(v_j) - f(p_\ell)}{1 - f(v_j) f(p_\ell)^*} \quad \text{and} \quad \text{Möb}_g \circ g(v_j) = \frac{g(v_j) - g(q_\ell)}{1 - g(v_j) g(q_\ell)^*},$$

respectively. For convenience, hereafter, we suppose the mappings f and g are the disk-shaped conformal parameterizations that satisfies $f(p_\ell) = 0$ and $g(q_\ell) = 0$, respectively, for some ℓ. The boundary mapping $h|_{\partial\mathbb{D}}$ is chosen to be the unique piecewise affine mapping that satisfies

$$\begin{cases} h \circ f\left(\gamma_{[p_d,p_{c+1}]}\right) = g\left(\gamma_{[q_d,q_{c+1}]}\right), \\ h \circ f\left(\gamma_{[p_{c+1},p_{c+2}]}\right) = g\left(\gamma_{[q_{c+1},q_{c+2}]}\right), \\ \qquad\qquad \vdots \\ h \circ f\left(\gamma_{[p_{d-1},p_d]}\right) = g\left(\gamma_{[q_{d-1},q_d]}\right). \end{cases} \tag{31}$$

8.2.2 Interior Registration Mapping

For convenience, we denote the discrete mappings by the vectors

$$\mathbf{h} = (h(v_1), \ldots, h(v_m))^\top \in \mathbb{C}^m \quad \text{and} \quad \mathbf{g} = (g(v_1), \ldots, g(v_n))^\top \in \mathbb{C}^n,$$

respectively, where $\mathbf{h}$ is unknown except boundary points. Let $\mathtt{P}$ and $\mathtt{Q}$ be the ordered sets of indices of the landmarks on $\mathcal{M}$ and $\mathcal{N}$, respectively. A smooth registration mapping (SRM) $h : \mathbb{D} \to \mathbb{D}$ is obtained by minimizing the *registration energy* defined as

$$\mathcal{E}_R(h) = \|L(h)\,\mathbf{h}\|_2^2 + \sum_{\ell=1}^{c} \lambda_\ell^2 |\mathbf{h}_{\mathtt{P}(\ell)} - \mathbf{g}_{\mathtt{Q}(\ell)}|^2 \tag{32}$$

in which λ_ℓ is an appropriate weight for the landmark pair $\left(\mathbf{h}_{\mathtt{P}(\ell)}, \mathbf{g}_{\mathtt{Q}(\ell)}\right)$, for $\ell = 1, \ldots, c$, $L(h)$ is the Laplacian matrix similar as in (14) defined by

$$[L(h)]_{i,j} = \begin{cases} -w_{i,j}(h) & \text{if } [v_i, v_j] \in \mathcal{E}(\mathcal{M}), \\ \sum_{\ell \neq i} w_{i,\ell}(h) & \text{if } j = i, \\ 0 & \text{otherwise}, \end{cases} \tag{33}$$

where $w_{i,j}(h)$ is the cotangent weight defined as

$$w_{i,j}(h) = \frac{\cot(\alpha_{i,j}(h)) + \cot(\alpha_{j,i}(h))}{2}$$

with $\alpha_{i,j}(h)$ and $\alpha_{j,i}(h)$ being two angles opposite to the edge $h([v_i, v_j])$ connecting points $h(v_i)$ and $h(v_j)$ on $\mathbb{C}$.

The surface registration process is performed as follows. First, an initial mapping $\mathbf{h}^{(0)}$ is computed by a harmonic mapping

$$[L(f)]_{\mathtt{I},\mathtt{I}}\mathbf{h}_{\mathtt{I}}^{(0)} = -[L(f)]_{\mathtt{I},\mathtt{B}}\mathbf{h}_{\mathtt{B}}^{(0)},$$

where f is given in (30), $\mathtt{I}$ and $\mathtt{B}$ denote the index sets of interior vertices and boundary vertices of $\mathcal{M}$, respectively. The given boundary condition $\mathbf{h}_{\mathtt{B}}^{(0)}$ is introduced in Sect. 8.2.1. Then the registration energy (32) is minimized by the iterative procedure

$$\mathbf{h}^{(k+1)} = \underset{\mathbf{h}_{\mathtt{B}}=\mathbf{h}_{\mathtt{B}}^{(0)}}{\operatorname{argmin}} \left(\left\| L(h^{(k)})\,\mathbf{h} \right\|_2^2 + \|\Lambda(\mathbf{h}_{\mathtt{P}} - \mathbf{g}_{\mathtt{Q}})\|_2^2 \right), \tag{34}$$

where Λ is the diagonal matrix with the diagonal entry $\Lambda_{\ell,\ell} = \lambda_\ell$, for $\ell = 1, \ldots, c$. The algorithm for computing the SRM is summarized in Algorithm 2.

Algorithm 2 Smooth Registration Mapping (SRM)

Input: Two simply connected open meshes $\mathcal{M}$ and $\mathcal{N}$, two index sets of landmark pairs $\mathtt{P}$ and $\mathtt{Q}$, and the weights for the landmark pairs λ_ℓ, for $\ell = 1, \ldots, d$.

Output: A registration mapping $\varphi : \mathcal{M} \to \mathcal{N}$.

1: Compute the conformal parameterizations $\mathbf{f}$ and $\mathbf{g}$ of the meshes $\mathcal{M}$ and $\mathcal{N}$, respectively, using the CEM algorithm [29].

2: Perform the Möbius transformations

$$\mathbf{f}_j \leftarrow \frac{\mathbf{f}_j - \mathbf{f}_{\mathtt{P}(\ell)}}{1 - \mathbf{f}_j \mathbf{f}_{\mathtt{P}(\ell)}^*} \quad \text{and} \quad \mathbf{g}_j \leftarrow \frac{\mathbf{g}_j - \mathbf{g}_{\mathtt{Q}(\ell)}}{1 - \mathbf{g}_j \mathbf{g}_{\mathtt{Q}(\ell)}^*},$$

for some ℓ.

3: Compute the unique piecewise affine mapping $\mathbf{h}_{\mathtt{B}}$ that satisfies (31).

4: Compute the initial mapping by

$$[L(f)]_{\mathtt{I},\mathtt{I}}\mathbf{h}_{\mathtt{I}} = -[L(f)]_{\mathtt{I},\mathtt{B}}\mathbf{h}_{\mathtt{B}}.$$

5: **while** not convergent **do**

6: Update $\mathbf{h}_{\mathtt{I}}$ by solving

$$\mathbf{h} \leftarrow \underset{\mathbf{h}_{\mathtt{B}}:\text{fixed}}{\operatorname{argmin}} \left(\|L(h)\,\mathbf{h}\|_2^2 + \|\Lambda(\mathbf{h}_{\mathtt{P}} - \mathbf{g}_{\mathtt{Q}})\|_2^2 \right).$$

7: **end while**

8: The desired registration mapping is $\varphi := g^{-1} \circ h \circ f$.

In practice, the surfaces we considered are the meshes of human faces captured by the 3D scanner *GeoVideo*. The coefficients λ_ℓ, $\ell = 1, \ldots, m$, in (32) are chosen to be 1. Fig. 14 (a), (c) and (e) show the models of *Lin Neutral*, *Lin Sad* and

Lin Pouting, respectively. Fig. 14 (b) shows the conformal parameterization of the model of *Lin Neutral* computed using the CEM algorithm [29]. Fig. 14 (d) and (f) show the registration mappings of *Lin Sad* and *Lin Pouting* computed by the SRM algorithm, respectively, where the target surface is *Lin Neutral*. The checkerboard patterns in Fig. 14 show the correspondence between each surface via the computed registration mapping.

The bijectivity of the registration mapping obtained by the SRM algorithm is, in general, not guaranteed. However, several experiments indicate that the registration mappings between meshes of human faces of different facial expressions are usually bijective, and the distortions of the mappings between the selected landmark pairs are very small. The reason is that the locations of each landmark pair on the parameterizations of human faces are usually similar so that the bijectivity is preserved under small deformations. However, the SRM algorithm would fail to produce a bijective registration mapping when the deformation is large. To overcome this issue, in the next subsection, we generalized the proposed SRM algorithm to dealing with the registration problem of large deformations.

8.2.3 Smooth Registration Mapping for Large Deformation

Given a set of landmark pairs on the disk $\{(p_\ell, q_\ell) \,|\, p_\ell \in \mathbb{D}, q_\ell \in \mathbb{D}\}_{\ell=1}^{d}$, where $|p_\ell - q_\ell|$ might be large. The problem is to find a smooth bijective mapping $h : \mathbb{D} \to \mathbb{D}$ such that

$$\begin{cases} h(p_\ell) = q_\ell, & \text{for } \ell = 1, \ldots, d, \\ h\,|_{\partial\mathbb{D}} = \mathrm{id}\,|_{\partial\mathbb{D}}\,, \end{cases} \tag{35}$$

where $\mathrm{id}\,|_{\partial\mathbb{D}}$ denotes the identity mapping on the boundary of the disk. Recall that the mapping can be computed by Algorithm 2 when the landmark pairs are close enough, i.e.,

$$\max_{\ell} |p_\ell - q_\ell| < \varepsilon$$

for some small value ε. To deal with the case that $|p_1 - q_1|, \ldots, |p_d - q_d|$ are relatively large, we apply the homotopy method. For each landmark pair (p_ℓ, q_ℓ), $\ell = 1, \ldots, d$, we suppose a continuous path $\gamma_\ell : [0, 1] \to \mathbb{D}$ is given such that $\gamma_\ell(0) = p_\ell$ and $\gamma_\ell(1) = q_\ell$. Assume each pair of paths does not intersect, i.e., $\gamma_i((0, 1)) \cap \gamma_j((0, 1)) = \varnothing$, for $i \neq j$. Given a sufficiently fine partition $0 = t_0 < t_1 < \cdots < t_N = 1$ of the interval $[0, 1]$ such that

$$|\gamma_\ell(t_{s-1}) - \gamma_\ell(t_s)| < \varepsilon,$$

for $s = 1, \ldots, N$. A registration problem of large deformations (35) is reduced into N registration problems of small deformations

$$\begin{cases} h_{t_{s-1}} \circ \gamma_\ell(t_{s-1}) = \gamma_\ell(t_s), & \text{for } \ell = 1, \ldots, d, \\ h_{t_{s-1}}\,|_{\partial\mathbb{D}} = \mathrm{id}\,|_{\partial\mathbb{D}}\,, \end{cases} \tag{36}$$

for $s = 1, \ldots, N$. Similar as (34), each registration problem can be solved iteratively by

$$\mathbf{h}_{t_{s-1}}^{(k+1)} = \underset{\mathbf{h}_{\mathrm{B}} = \mathbf{h}_{\mathrm{B}}^{(0)}}{\operatorname{argmin}} \left(\left\| L(h_{t_{s-1}}^{(k)})\,\mathbf{h} \right\|_2^2 + \sum_{\ell=1}^{d} |h \circ \gamma_\ell(t_{s-1}) - \gamma_\ell(t_s)|^2 \right), \tag{37}$$

where $\mathtt{B}$ denotes the index set of the boundary vertices. Then the desired registration mapping that satisfies (35) is given by

$$h := h_{t_N} \circ h_{t_{N-1}} \circ \cdots \circ h_{t_0}.$$

The algorithm for computing the SRM for large deformations (SRMLD) is summarized in Algorithm 3.

Algorithm 3 Smooth Registration Mapping for Large Deformation (SRMLD)

Input: A mesh $\mathcal{M}$ of the unit disk with vertices $v_1, \ldots, v_n$, an index set of landmarks $\mathtt{P}$ and a set of landmark on the disk $\{q_\ell \in \mathbb{D}\}_{\ell=1}^d$ together with a set of continuous paths

$$\left\{\gamma_\ell : [0,1] \to \mathbb{D} \,\middle|\, \gamma_\ell(0) = v_{\mathtt{P}(\ell)}, \gamma_\ell(1) = q_\ell \right\}_{\ell=1}^d,$$

and a partition

$$0 = t_0 < t_1 < \cdots < t_N = 1$$

of the interval $[0,1]$.

Output: A smooth bijective mapping $h : \mathbb{D} \to \mathbb{D}$ such that

$$\begin{cases} h(v_{\mathtt{P}(\ell)}) = q_\ell, & \text{for } \ell = 1, \ldots, d, \\ h\,|_{\partial\mathbb{D}} = \mathrm{id}\,|_{\partial\mathbb{D}}\,. \end{cases}$$

1: Set $\mathbf{h} = (v_1, \ldots, v_n)^\top \in \mathbb{C}^n$.
2: **for** $s = 1, \ldots, N$ **do**
3: Set $\mathbf{g}_\ell = \gamma_\ell(t_s)$, for $\ell = 1, \ldots, d$.
4: **while** not convergent **do**
5: Update $\mathbf{h}_\mathtt{I}$ by solving

$$\mathbf{h} \leftarrow \underset{\mathbf{h}_\mathtt{B}:\text{fixed}}{\operatorname{argmin}} \left(\|L(h)\,\mathbf{h}\|_2^2 + \|\mathbf{h}_\mathtt{P} - \mathbf{g}\|_2^2 \right).$$

6: **end while**
7: **end for**

Fig. 13 shows some examples of deformation fields by Algorithm 3. The locations of red dots are mapped to the locations of blue circles by the registration mapping. The black arrows indicate the inputted paths. It is worth noting that the registration mappings demonstrated in Fig. 13 are bijective.

Remark 5 In general, the bijectivity of the proposed SRMLD algorithm is guaranteed under the assumption that there exists an $\varepsilon > 0$ such that for every possible set of landmark pairs $\{(p_\ell, q_\ell) \,|\, p_\ell \in \mathbb{D}, q_\ell \in \mathbb{D}\}_{\ell=1}^d$ with $\max_\ell |p_\ell - q_\ell| < \varepsilon$, the iteration (34) is bijectivity-preserving.

8.3 Surface Morphing via Registration Mappings

A *morphing* between two surfaces refers to the continuous deformation history from one surface to another one [19,28]. In this subsection, we demonstrate the computational procedure for the construction of the morphing between surfaces.

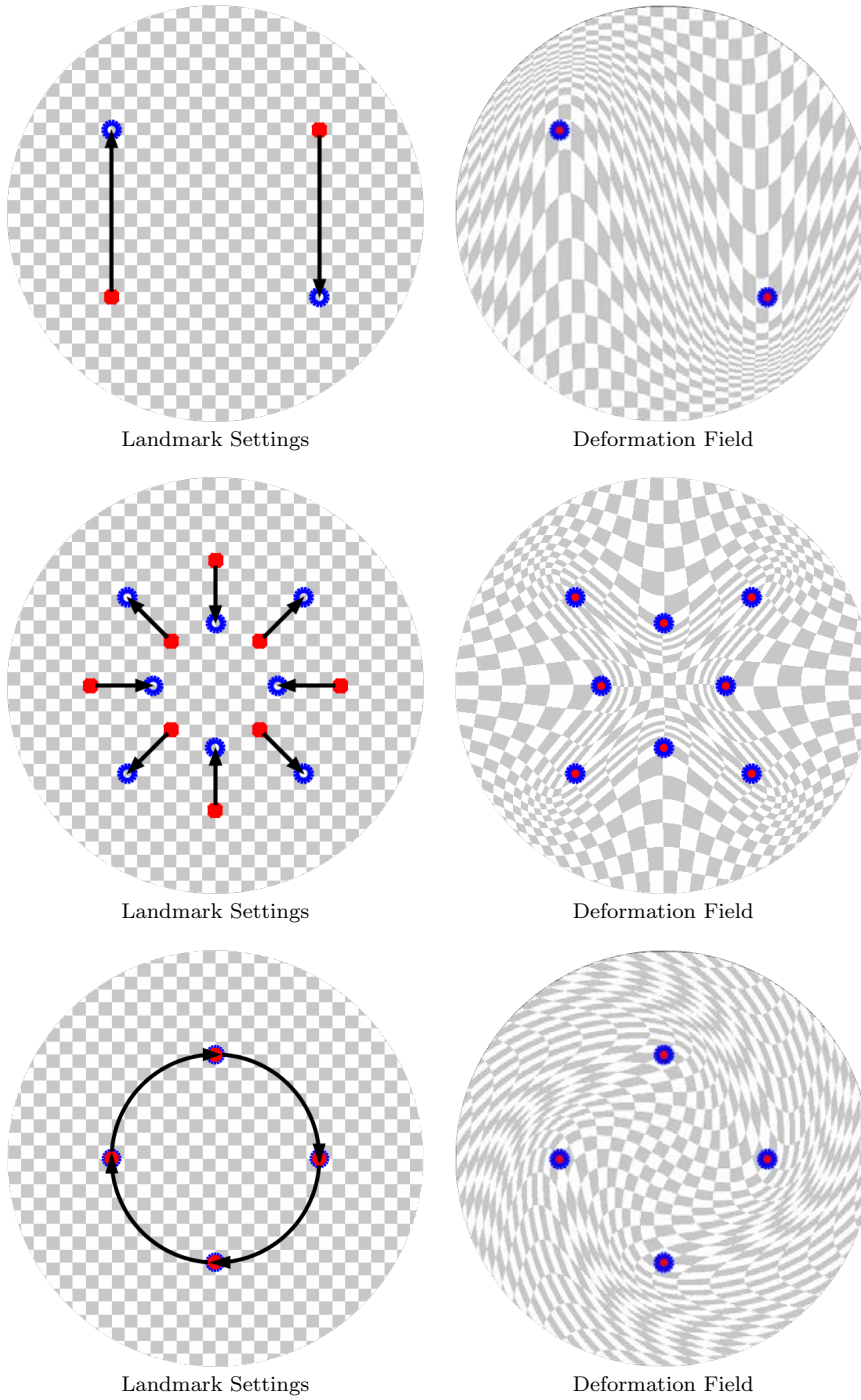

Fig. 13 The landmark settings (left) and the deformation field (right) by the SRMLD algorithm. The locations of red dots are mapped to the locations of blue circles by the registration mappings. The black arrows indicate the inputted paths.

Given two surfaces $\mathcal{M}_0$, $\mathcal{M}_1$ and a registration mapping $\varphi_1 : \mathcal{M}_0 \to \mathcal{M}_1$ obtained by Algorithm 2. A morphing between surfaces can be carried out by applying the linear homotopy $\mathcal{H} : [0,1] \times \mathcal{M}_0 \to \mathbb{R}^3$ defined by

$$\mathcal{H}(t,v) = (1-t)v + t\,\varphi_1(v).$$

In general, suppose $T+1$ surfaces $\mathcal{M}_0, \ldots, \mathcal{M}_T$ and registration mappings $\varphi_\ell : \mathcal{M}_0 \to \mathcal{M}_\ell$, $\ell = 1, \ldots, T$, are given. A desired morphing between these surfaces can be computed by choosing a suitable homotopy $\mathcal{H} : [0,T] \times \mathcal{M}_0 \to \mathbb{R}^3$ that satisfies

$$\mathcal{H}(t,v) = \varphi_t(v),$$

for $t = 1, \ldots, T$, which can be carried out by the interpolation between the data points

$$\{(0,v), (1,\varphi_1(v)), \ldots, (T,\varphi_T(v)) \mid v \in \mathcal{M}_0\}.$$

Here we adopt the *piecewise cubic Hermite interpolating polynomial* [14] to obtain a smooth path of homotopy so that the morphing looks more natural. A demo video of surface morphing between facial expressions via the registration mappings can be found at https://mhyueh.github.io/projects/DiskmapSEM.html.

9 Concluding Remarks

In this paper, we mainly propose a novel efficient SEM algorithm for the computation of equiareal parameterizations of simply connected open surfaces. The demonstrated numerical results of the SEM algorithm has the following advantages:

- **Highly Improved Robustness**: For every demonstrated mesh models, the iteration of the SEM algorithm converges and produces a reasonably good equiareal parameterization.
- **Highly Improved Effectiveness**: The effectiveness of the proposed SEM algorithm outperforms other state-of-the-art algorithms [27, 25]. Numerical results indicate that an equiareal parameterization by the SEM algorithm can be computed in less than 3 seconds for a mesh model of more than 100,000 triangular faces.
- **Small Area Distortion**: For every demonstrated numerical result, the total area distortion is less than 5%, which outperforms other state-of-the-art algorithms [27, 25].

Thanks to the robustness of the proposed algorithm, the computation of the surface remeshing, surface registration and surface morphing can be performed efficiently and reliably.

Acknowledgements

The authors want to thank Prof. Xianfeng David Gu for the useful discussion and the executable program files of the OMT algorithm. This work is partially supported by the Ministry of Science and Technology, the National Center for Theoretical Sciences, the Taida Institute for Mathematical Sciences, the ST Yau

Fig. 14 (a) The model of *Lin Neutral*. (b) The conformal parameterization obtained by CEM algorithm. (c) The model of *Lin Sad*. (d) The registration mapping obtained by SRM algorithm. (e) The model of *Lin Pouting*. (f) The registration mapping obtained by SRM algorithm.

Center at NCTU, and the Center of Mathematical Sciences and Applications at Harvard University. This work is supported in part by the Ministry of Science and Technology, Taiwan, Republic of China, under Grant MOST 106-2811-M-009-046.

References

1. ALICE. http://alice.loria.fr/.
2. David Xianfeng Gu's Home Page. http://www3.cs.stonybrook.edu/~gu/.
3. Digital Shape Workbench - Shape Repository. http://visionair.ge.imati.cnr.it/ontologies/shapes/.
4. The Stanford 3D Scanning Repository. http://graphics.stanford.edu/data/3Dscanrep/.
5. TurboSquid. http://www.turbosquid.com/.
6. P. Alliez, G. Ucelli, C. Gotsman, and M. Attene. *Recent Advances in Remeshing of Surfaces*, pages 53–82. Springer Berlin Heidelberg, Berlin, Heidelberg, 2008.
7. A. Berman and R. Plemmons. *Nonnegative Matrices in the Mathematical Sciences*. Society for Industrial and Applied Mathematics, 1994.
8. S.-W. Cheng, T. K. Dey, and J. Shewchuk. *Delaunay Mesh Generation*. Chapman & Hall/CRC, 1st edition, 2012.
9. C. P. Choi, X. Gu, and L. M. Lui. Subdivision connectivity remeshing via Teichmüller extremal map. *Inverse Probl. Imag.*, 11(1930-8337_2017_5_825):825, 2017.
10. P. T. Choi, K. C. Lam, and L. M. Lui. FLASH: Fast landmark aligned spherical harmonic parameterization for genus-0 closed brain surfaces. *SIAM J. Imaging Sci.*, 8(1):67–94, 2015.
11. A. Dominitz and A. Tannenbaum. Texture mapping via optimal mass transport. *IEEE T. Vis. Comput. Graph.*, 16(3):419–433, May 2010.
12. M. S. Floater. Parametrization and smooth approximation of surface triangulations. *Computer Aided Geometric Design*, 14(3):231 – 250, 1997.
13. M. S. Floater and K. Hormann. Surface parameterization: a tutorial and survey. *Math. Visual.*, pages 157–186, 2005.
14. F. N. Fritsch and R. E. Carlson. Monotone piecewise cubic interpolation. *SIAM J. Numer. Anal.*, 17(2):238–246, 1980.
15. X. Gu, F. Luo, J. Sun, and S.-T. Yau. Variational principles for Minkowski type problems, discrete optimal transport, and discrete Monge-Ampere equations. arXiv:1302.5472 [math.GT].
16. K. Hormann, B. Lévy, and A. Sheffer. Mesh parameterization: Theory and practice. In *ACM SIGGRAPH Course Notes*, 2007.
17. R. A. Horn and C.R. Johnson. *Matrix Analysis*. Cambridge University Press, 1990.
18. K. C. Lam and L. M. Lui. Landmark- and intensity-based registration with large deformations via quasi-conformal maps. *SIAM J. Imaging Sci.*, 7(4):2364–2392, 2014.
19. K. C. Lam, C. Wen, and L. M. Lui. Conformal-based surface morphing and multi-scale representation. *Axioms*, 3(2):222–243, 2014.
20. L. M. Lui, K. C. Lam, S.-T. Yau, and X. Gu. Teichmuller mapping (t-map) and its applications to landmark matching registration. *SIAM J. Imaging Sci.*, 7(1):391–426, 2014.
21. J. J. Molitierno. *Applications of Combinatorial Matrix Theory to Laplacian Matrices of Graphs*. CRC Press, 2012.
22. S. Nadeem, Z. Su, W. Zeng, A. Kaufman, and X. Gu. Spherical parameterization balancing angle and area distortions. *IEEE T. Vis. Comput. Gr.*, 23(6):1663–1676, June 2017.
23. P. V. Sander, J. Snyder, S. J. Gortler, and H. Hoppe. Texture mapping progressive meshes. In *Proceedings of the 28th Annual Conference on Computer Graphics and Interactive Techniques*, SIGGRAPH '01, pages 409–416, New York, NY, USA, 2001. ACM.
24. A. Sheffer, E. Praun, and K. Rose. Mesh parameterization methods and their applications. *Found. Trends. Comp. Graphics and Vision.*, 2(2):105–171, 2006.
25. K. Su, L. Cui, K. Qian, N. Lei, J. Zhang, M. Zhang, and X. D. Gu. Area-preserving mesh parameterization for poly-annulus surfaces based on optimal mass transportation. *Comput. Aided Geom. D.*, 46:76 – 91, 2016.
26. Y. Yoshiyasu, W.-C. Ma, E. Yoshida, and F. Kanehiro. As-conformal-as-possible surface registration. *Comput. Graph. Forum*, 33(5):257–267, August 2014.

27. S. Yoshizawa, A. Belyaev, and H. P. Seidel. A fast and simple stretch-minimizing mesh parameterization. In *Proceedings Shape Modeling Applications, 2004.*, pages 200–208, June 2004.
28. M.-H. Yueh, X. D. Gu, W.-W. Lin, C.-T. Wu, and S.-T. Yau. Conformal surface registration with applications on face morphing. 2016. mathscidoc:1605.09001.
29. M.-H. Yueh, W.-W. Lin, C.-T. Wu, and S.-T. Yau. An efficient energy minimization for conformal parameterizations. *J. Sci. Comput.*, 73(1):203–227, Oct 2017.
30. X. Zhao, Z. Su, X. D. Gu, A. Kaufman, J. Sun, J. Gao, and F. Luo. Area-preservation mapping using optimal mass transport. *IEEE T. Vis. Comput. Gr.*, 19(12):2838–2847, Dec 2013.
31. G. Zou, J. Hu, X. Gu, and J. Hua. Authalic parameterization of general surfaces using Lie advection. *IEEE T. Vis. Comput. Graph.*, 17(12):2005–2014, December 2011.

A Derivations of Gradients of the Stretch Energy

In this section, we derive the explicit formulas (17) and (18) for the gradients of the stretch energy.

Proposition 1 *Given a mesh $\mathcal{M}$ of n vertices and a bijective piecewise affine mapping $f : \mathcal{M} \to \mathcal{D} \subset \mathbb{C}$. Let $\mathbf{f} = (f(v_1), \ldots, f(v_n))^\top$ and $L(\mathbf{f})$ be defined as (14). Suppose $[v_j, v_k] \in \mathcal{E}(\mathcal{M})$. Then Eq. (17) holds, for $s = 1, 2$.*

Proof For each edge $[v_j, v_k] \in \mathcal{E}(\mathcal{M})$,

$$\begin{aligned}
\left[(\mathbf{f}^s)^\top \frac{\partial L(\mathbf{f})}{\partial \mathbf{f}^s}\right]_{j,k} &= \sum_{\alpha=1}^{n} \mathbf{f}_\alpha^s \frac{\partial L_{\alpha,j}}{\partial \mathbf{f}_k^s} = \sum_{\alpha\neq j,k} \mathbf{f}_\alpha^s \frac{\partial L_{\alpha,j}}{\partial \mathbf{f}_k^s} + \mathbf{f}_j^s \frac{\partial L_{j,j}}{\partial \mathbf{f}_k^s} + \mathbf{f}_k^s \frac{\partial L_{k,j}}{\partial \mathbf{f}_k^s} \\
&= \sum_{\alpha\neq j,k} (\mathbf{f}_\alpha^s - \mathbf{f}_j^s) \frac{\partial L_{\alpha,j}}{\partial \mathbf{f}_k^s} + (\mathbf{f}_k^s - \mathbf{f}_j^s) \frac{\partial L_{k,j}}{\partial \mathbf{f}_k^s} \\
&= -\frac{1}{2} \sum_{[v_\alpha, v_j, v_k] \in \mathcal{F}(\mathcal{M})} (\mathbf{f}_\alpha^s - \mathbf{f}_j^s) \frac{2\mathbf{f}_k^s - \mathbf{f}_\alpha^s - \mathbf{f}_j^s}{2|[v_i, v_j, v_k]|} \\
&\quad - \frac{1}{2} (\mathbf{f}_k^s - \mathbf{f}_j^s) \sum_{[v_\alpha, v_j, v_k] \in \mathcal{F}(\mathcal{M})} \frac{\mathbf{f}_j^s - \mathbf{f}_\alpha^s}{2|[v_\alpha, v_j, v_k]|} \\
&= -\frac{1}{2} \sum_{[v_\alpha, v_j, v_k] \in \mathcal{F}(\mathcal{M})} \frac{(\mathbf{f}_k^s - \mathbf{f}_\alpha^s)(\mathbf{f}_\alpha^s - \mathbf{f}_j^s)}{2|[v_\alpha, v_j, v_k]|}.
\end{aligned}$$

On the other hand, the diagonal entries

$$\begin{aligned}
\left[(\mathbf{f}^s)^\top \frac{\partial L(\mathbf{f})}{\partial \mathbf{u}^s}\right]_{j,j} &= \sum_{\alpha=1}^{n} \mathbf{f}_\alpha^s \frac{\partial L_{\alpha,j}}{\partial \mathbf{f}_j^s} = \sum_{\alpha\neq j} \mathbf{f}_\alpha^s \frac{\partial L_{\alpha,j}}{\partial \mathbf{f}_j^s} + \mathbf{f}_j^s \frac{\partial L_{j,j}}{\partial \mathbf{f}_j^s} = \sum_{\alpha\neq j} (\mathbf{f}_\alpha^s - \mathbf{f}_j^s) \frac{\partial L_{\alpha,j}}{\partial \mathbf{f}_j^s} \\
&= -\frac{1}{2} \sum_{\alpha\neq j} (\mathbf{f}_\alpha^s - \mathbf{f}_j^s) \sum_{[v_\alpha, v_j, v_\beta] \in \mathcal{F}(\mathcal{M})} \frac{\mathbf{f}_\alpha^s - \mathbf{f}_\beta^s}{2|[v_\alpha, v_j, v_\beta]|} \\
&= -\frac{1}{2} \sum_{[v_\alpha, v_j, v_\beta] \in \mathcal{F}(\mathcal{M})} \frac{(\mathbf{f}_\alpha^s - \mathbf{f}_\beta^s)^2}{2|[v_\alpha, v_j, v_\beta]|}.
\end{aligned}$$

□

Proposition 2 *Given a mesh $\mathcal{M}$ of n vertices and a bijective piecewise affine mapping $f : \mathcal{M} \to \mathcal{D} \subset \mathbb{C}$. Let $\mathbf{f} = (f(v_1), \ldots, f(v_n))^\top$ and $L(\mathbf{f})$ be defined as (14). Suppose $[v_j, v_k] \in \mathcal{E}(\mathcal{M})$. Then Eq. (18) holds, for $(s,t) = (1,2), (2,1)$.*

Proof For each edge $[v_j, v_k] \in \mathcal{E}(\mathcal{M})$,

$$\begin{aligned}
\left[(\mathbf{f}^s)^\top \frac{\partial L(\mathbf{f})}{\partial \mathbf{f}^t}\right]_{j,k} &= \sum_{\alpha=1}^{n} \mathbf{f}_\alpha^s \frac{\partial L_{\alpha,j}}{\partial \mathbf{f}_k^t} = \sum_{\alpha\neq j,k} \mathbf{f}_\alpha^s \frac{\partial L_{\alpha,j}}{\partial \mathbf{f}_k^t} + \mathbf{f}_j^s \frac{\partial L_{j,j}}{\partial \mathbf{f}_k^t} + \mathbf{f}_k^s \frac{\partial L_{k,j}}{\partial \mathbf{f}_k^t} \\
&= \sum_{\alpha\neq j,k} (\mathbf{f}_\alpha^s - \mathbf{f}_j^s) \frac{\partial L_{\alpha,j}}{\partial \mathbf{f}_k^s} + (\mathbf{f}_k^s - \mathbf{f}_j^s) \frac{\partial L_{k,j}}{\partial \mathbf{f}_k^s} \\
&= -\frac{1}{2} \sum_{[v_\alpha, v_j, v_k] \in \mathcal{F}(\mathcal{M})} (\mathbf{f}_\alpha^s - \mathbf{f}_j^s) \frac{2\mathbf{f}_k^t - \mathbf{f}_\alpha^t - \mathbf{f}_j^t}{2|[v_i, v_j, v_k]|} \\
&\quad - \frac{1}{2} (\mathbf{f}_k^s - \mathbf{f}_j^s) \sum_{[v_\alpha, v_j, v_k] \in \mathcal{F}(\mathcal{M})} \frac{\mathbf{f}_j^t - \mathbf{f}_\alpha^t}{2|[v_\alpha, v_j, v_k]|} \\
&= -\frac{1}{2} \sum_{[v_\alpha, v_j, v_k] \in \mathcal{F}(\mathcal{M})} \frac{2(\mathbf{f}_k^s - \mathbf{f}_\alpha^s)(\mathbf{f}_\alpha^t - \mathbf{f}_j^t) - (\mathbf{f}_j^s - \mathbf{f}_\alpha^s)(\mathbf{f}_\alpha^t - \mathbf{f}_k^t)}{2|[v_\alpha, v_j, v_k]|}.
\end{aligned}$$

On the other hand, the diagonal entries

$$\begin{aligned}
\left[(\mathbf{f}^s)^\top \frac{\partial L(\mathbf{f})}{\partial \mathbf{f}^t}\right]_{j,j} &= \sum_{\alpha=1}^{n} \mathbf{f}_\alpha^s \frac{\partial L_{\alpha,j}}{\partial \mathbf{f}_j^t} = \sum_{\alpha\neq j} \mathbf{f}_\alpha^s \frac{\partial L_{\alpha,j}}{\partial \mathbf{f}_j^t} + \mathbf{f}_j^s \frac{\partial L_{j,j}}{\partial \mathbf{f}_j^t} = \sum_{\alpha\neq j} (\mathbf{f}_\alpha^s - \mathbf{f}_j^s) \frac{\partial L_{\alpha,j}}{\partial \mathbf{f}_j^t} \\
&= -\frac{1}{2} \sum_{\alpha\neq j} (\mathbf{f}_\alpha^s - \mathbf{f}_j^s) \sum_{[v_\alpha, v_j, v_\beta] \in \mathcal{F}(\mathcal{M})} \frac{\mathbf{f}_\alpha^t - \mathbf{f}_\beta^t}{2|[v_\alpha, v_j, v_\beta]|} \\
&= -\frac{1}{2} \sum_{[v_\alpha, v_j, v_\beta] \in \mathcal{F}(\mathcal{M})} \frac{(\mathbf{f}_\alpha^s - \mathbf{f}_\beta^s)(\mathbf{f}_\alpha^t - \mathbf{f}_\beta^t)}{2|[v_\alpha, v_j, v_\beta]|}.
\end{aligned}$$

□